Comparison of geophysical techniques to determine depth to bedrock in complex weathered environments of the Mount Crawford region, South Australia

Thomas James Fotheringham
November 2013

THE UNIVERSITY
of ADELAIDE

COMPARISON OF GEOPHYSICAL TECHNIQUES TO DETERMINE DEPTH TO BEDROCK IN COMPLEX WEATHERED ENVIRONMENTS OF THE MOUNT CRAWFORD REGION, SOUTH AUSTRALIA

GEOPHYSICAL COMPARISON OF BEDROCK DEPTH

ABSTRACT

Geophysical techniques have the ability to characterise the subsurface and define the depth to bedrock. The non-destructive nature and relatively cheap costs of geophysical surveying compared to drilling make it an attractive tool for subsurface analysis. Many studies have utilized geophysics to interpret soil features such as clay content, water content, salinity, textural properties and bulk density. Further work has been done to map the regolith-bedrock boundary. Previous work has been conducted in the Mount Crawford region using remote sensing based techniques to determine depth to bedrock. Comparisons between the effectiveness of different geophysical techniques at determining depth to bedrock have not previously been undertaken in similar environments. Fieldwork was undertaken along three transects chosen to represent different geological environments. Three geophysical apparatus were compared: Electrical Resistivity (ER), Frequency Domain EM (FDEM) and Ground Penetrating Radar (GPR). A simultaneous soil sampling program was conducted to provide ground truthing. The work in this study reveals the strengths and weakness of the three geophysical techniques at determining depth to bedrock in complex weathered environments of the Mount Crawford region, South Australia. The study reveals differences in the responses of the three geophysical techniques at each of the transects. The GPR was found to be largely unsuitable due to rapid attenuation of the signal. Resistivity and FDEM appeared to show similar variations in the models generated, with differences in the resolution and depth of investigation relating to intrinsic differences between the two systems. Qualitative analysis of the data suggests resistivity provides the strongest correlations with drill refusal depths. The FDEM appeared to display similar trends to the resistivity data and the system offers faster data acquisition, however the inverted model displays lower resolution. The data suggests that bedrock along the surveyed transects is highly weathered and relatively conductive compared to overlying regolith.

TABLE OF CONTENTS

LIST OF FIGURES AND TABLES (LEVEL 1 HEADING)

INTRODUCTION

Determining the depth to bedrock, as well as the soil characteristics of the shallow subsurface is difficult, due to the changes these undergo through space and time. There is a desire to be able to accurately identify shallow subsurface features using geophysics. Shallow geophysics has been used frequently to identify features in the regolith and reveal its contact with bedrock, as it provides a cheaper, less invasive method when compared to soil sampling programs. Improvements in data acquisition, processing and interpretation have seen a marked increase in the implementation of geophysical techniques.

Providing a method for locating the regolith-bedrock boundary that is cheaper and more time efficient than traditional surface based, drilling-based soil sampling programs has benefits to the industrial, environmental and agricultural industries. Wilford and Thomas (2012) conducted a study over much of the Mount Lofty Ranges, South Australia, using remote sensing techniques in conjunction with readily available data sets and statistical modelling to predict the depth to bedrock. The work conducted in this project is intended to supplement the information that remote sensing based studies can obtain, as well as act as a stand-alone technique for determining the depth to bedrock and characterising other important soil characteristics.

Electrical resistivity (ER) has been used to understand and map soil properties and processes, including salinity, soil nutrient content, textural properties (sand, clay, loam content etc), water content, subsurface water movement, temperature and bulk density (see Friedman 2005, Samouëlian et al. 2005, Paillet et al. 2010, Shafique et al. 2011, Badmus et al. 2012). ER has also been used to interpret depth to bedrock in a modern fluvial system in Taiwan (Hsu et al. 2010). Electromagnetic induction (EMI) has successfully been used to map soil

characteristics in Australia (Williams and Hoey 1987, Triantafilis et al. 2001, Triantafilis and Lesch 2005). Sudduth et al. (1995) undertook comparable work in the United States while Brus et al. (1992) conducted similar work in the Netherlands. Ground Penetrating Radar (GPR) has been used by Senechal et al. (2000) and De Benedetto et al. (2010) to help characterise soil properties, such as lateral continuities/discontinuities and clay content. De Benedetto et al. (2010) found that highly conductive soils, associated with high clay content, caused attenuation of the signal. While these techniques have often been run individually, they have not been tested and compared against each other, in this type of setting.

I propose that by running three relatively inexpensive geophysical surveys over an area it is possible to provide information on the depth to bedrock and identify shallow subsurface features. Ultimately, this could result in lowering the costs and reducing the number of drill-holes required to characterise an area. The work is carried out in the Mount Crawford region of the Mt Lofty Ranges, South Australia. By testing which technique (or a combination of techniques) is effective at characterising the regolith-bedrock contact it will allow for future tests to be conducted with more confidence and provide an auxiliary method for testing and predicting regolith thickness, leading to more efficient land use.

In this study three geophysical techniques are compared along three transects to establish which techniques provide effective data for determining the regolith-bedrock boundary. The three transects were selected by Mark Thomas and John Wilford to provide further information on their remote sensing based study of the region (Wilford and Thomas 2012). Results from the geophysical methods tested are compared with soil survey data collected concurrently through a drilling program conducted along the same transects. For the purpose of this work, bedrock will be interpreted as the depth of drill refusal. The effectiveness of

each technique will be directly comparable to the measured soil data, suggesting the environments where these techniques are suitable for bedrock determination. This provides insight into which technique to utilise in future geophysics based regolith surveys to maximise efficiency.

BACKGROUND AND GEOLOGY

Background

The Mount Crawford Forest Reserve is located in the central Mount Lofty Ranges, South Australia. The region hosts a range of geological units associated with the Adelaidean Sediments, as well as an anticlinal core of pre-Adelaidean Basement (Preiss et al. 2008). Data collection was carried out on three transects; Transect1 (Rocky Paddock), Transect2 (Chalkies) and Transect 3 (Canham Rd) as shown in Figure 1. The study area is subject to a Mediterranean climate, producing cool winters and hot, dry summers. This leads to seasonal rainfall, which is orographically influenced, with the higher elevation western side of the ranges experiencing more rainfall than the lower elevation eastern side. The study area is located in the central Mount lofty Ranges. Rainfall varies from 800-1100mm in the west down to 350-500mm in the east of the Ranges.
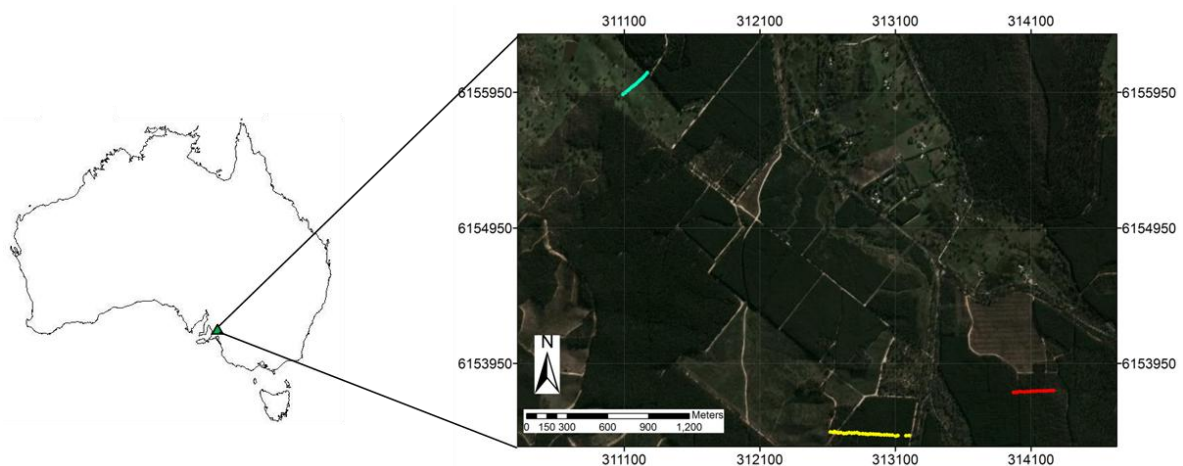
Figure 1: Location map of the study area is shown by the green triangle. The three transects, all of which are located within the Mount Crawford Forest region, South Australia are displayed on the satellite map image. Transect1 (Rocky Paddock) is represented by the blue line, transect 2 (Chalkies) by the red line and Transect 3 (Canham Rd) by the blue line. Eastings and northings (WGS 84, zone54S) are displayed for reference location.

Regional Geology

The region has a relatively complex geological history, having undergone both extensional and contractional deformation events. The Mount Lofty Ranges have undergone three principal neotectonic stages that are each associated with different tectonic regimes (Tokarev 2005). The first stage was an extensional stage that extended from the Middle Eocene-Middle Miocene. This was followed by a transitional stage from the Late Miocene-Early Pleistocene. The final stage is a compressional stage that has extended from the Early Pleistocene to the present.

During the early Cainozoic a large area of South Australia existed as a gently undulating and deeply weathered palaeoplain (Tokarev 2005). During this period sea level was changing, having a significant effect on the landscape. Initial crustal segmentation during the Middle-late Eocene involved subsidence of the St. Vincent and Western Murray Basins (McGowran 1989), while remnants of the high-standing palaeoplain became the Mount Lofty Ranges (Tokarev 2005). Embayments and intramontane basins, such as the Meadows-Myponga, Hindmarsh Tiers and Barossa were formed from further crustal segmentation(Lindsay and Alley 1995). Accommodation zones, strain transfer, tilting and crustal segmentation are all recognised as fundamental attributes to the extensional tectonic setting of this time (Tokarev 2005).

Major compressional tectonic activity in the region was associated with steep angle reverse faulting on both sides of the Mount Lofty ranges (Tokarev 2005). The compression associated with this event led to uplift of the Mount Lofty ranges during the Pleistocene that resulted in a major lithological change in the sediments of the St Vincent and Western

Murray Basins (Tokarev 2005). This period of compression remains ongoing since the Pleistocene and can be seen today through the seismic activity of the ranges (Tokarev 2005).

Local Geology

The Mount Crawford Region is a geologically complex zone in the Adelaidean Sediments that make up the Mount Lofty Ranges (Preiss et al. 2008). It is located within a high-grade (amphibolite facies) suite of rocks that are located to the east of the Williamstown-Meadows Fault (Preiss et al. 2008). The region contains an anticlinal core of pre-Adelaidean basement that is only otherwise exposed in the high grade, small and poorly exposed Oakbank Inlier (Preiss et al. 2008). The Mount Crawford region also contains the Aldgate Sandstone, which in this location trends eastwards, into a major east dipping shear zone (Preiss et al. 2008). The variation in geological units within the Mt Crawford region allows for significant change in lithologies over a small area.

Data were collected along the three transects, each chosen to represent a different geological environment of the Mount Crawford Region.

TRANSECT 1: ROCKY PADDOCK
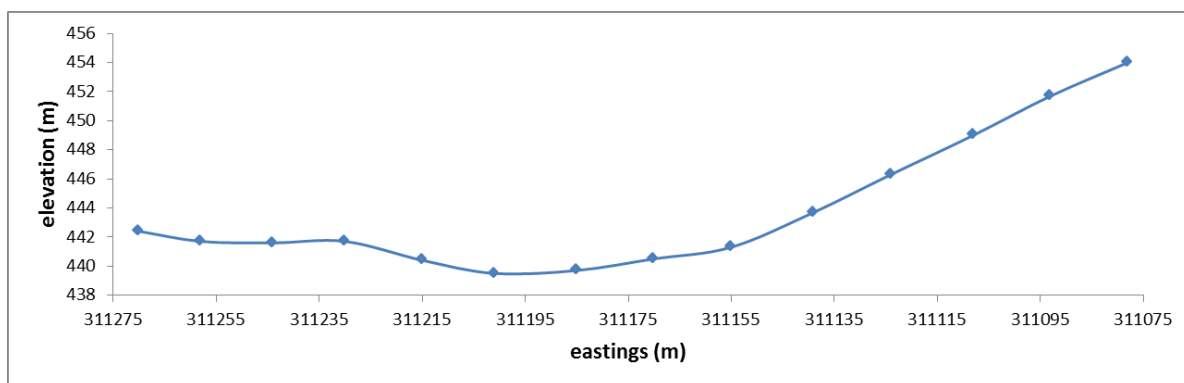
Figure 2: Topography of the Rocky Paddock transect generated from differential GPS data collected at each of the drill-holes (shown by diamonds) along the transect. The data have been smoothed. The transect was orientated in a northeast-southwest direction, with geophysical surveying and drilling starting at the north-eastern end of the transect.

Transect 1 (Rocky Paddock) is located on private farmland. The terrain consists of open paddocks occupied by sheep and alpaca. There is sparsely scattered tree cover. Transect 1 is orientated in a northeast-southwest direction, with drilling and geophysical surveying conducted in the same direction. The topography profile of Transect 1 can be seen in Figure 2. Transect 1 crosses a geological boundary, where the rocks change from gneissic in the south-west (the first 100m) to schistose in the north-eastern end of the transect. Subcrop/outcrop is present in the lowest regions of Transect 1.

TRANSECT 2: CHALKIES
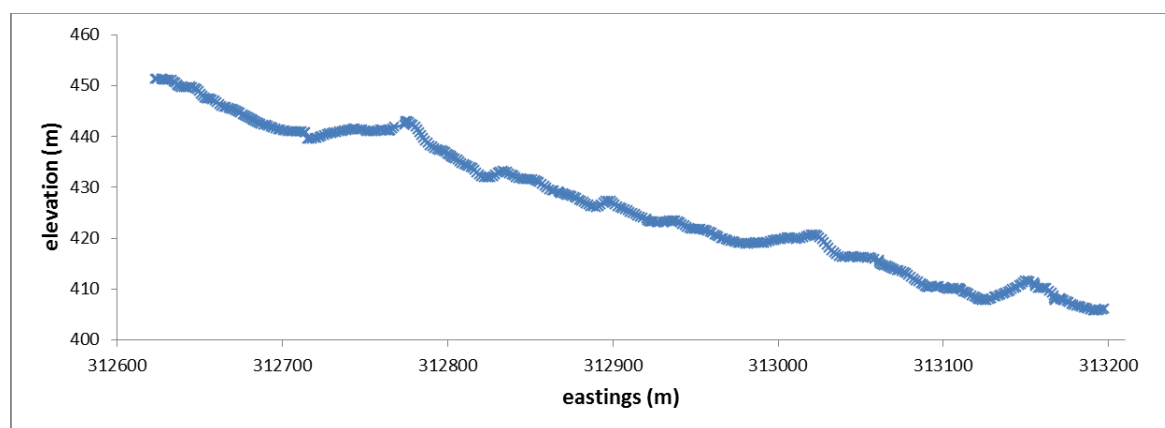
Figure 3: Topography of Chalkies transect generated from differential GPS data. The data have had a 5 point smoothing filter applied. Geophysical surveying and drilling was conducted in a west to east direction.

Transect 2 (Chalkies) is located on a gradual eastward facing slope. There is approximately 50m of relief along Transect 2 (Figure 3). It contains one notable rise in topography between eastings 312710 and 312780. It is orientated in an west-east direction, with geophysical surveying and drilling carried out in a west-east direction. The transect is dominated by thick clays and fine grained micaceous sediments, underlain by schistose and quartz sandstone dominated bedrock. Drilling and geophysical surveying was conducted off the side of a forest track, and it crossed another forest track between eastings 312660 and 312680. The first 50 metres were located in native vegetation, with the remainder surrounded on both sides by *Pinus radiata* forest.

TRANSECT 3: CANHAM RD
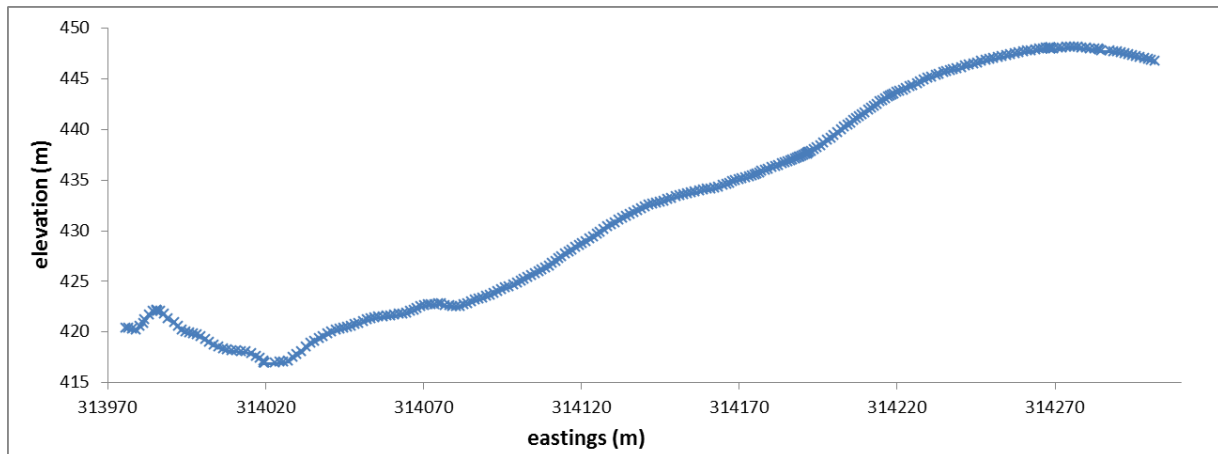
Figure 4: Topography of the Canham Rd transect generated from differential GPS data. The data have had a 5 point smoothing filter applied. Geophysical surveying was carried out in an east to west direction, while drilling was conducted in a west to east direction.

Transect 3 (Canham Rd) has considerable variation in topography as shown in Figure 4. The transect is orientated in an east-west direction. Geophysical surveying was carried out in an east-west direction, whilst drilling was conducted in a west-east direction. The eastern 100 metres is dominated by ferruginous, highly weathered quartz sandstones and was surrounded by native vegetation. Transect 3 then shifts to thicker clay cover, with one side of the transect bound by *Pinus radiata* forest. There were several intersecting roads that appeared to drain into the lower regions of the transect.

METHODS AND THEORY

Electrical Resistivity method

Resistivity surveys work by transmitting a direct current into the ground and measuring the resulting potential differences at different locations on the ground surface (Samouëlian et al. 2005). The patterns of the potential difference allow information to be gathered on the shapes, distributions and electrical properties of subsurface heterogeneities (Samouëlian et al. 2005).

The resistivity ρ (given in Ωm) of a simple cylindrical body is defined as:

$$\rho = R \cdot \left(\frac{S}{L}\right)$$ (1)

Where R is the electrical resistance (Ω), L the length of the cylinder (m) and S represents the cylinders cross-sectional area (m^2).

The cylindrical body's electrical resistance R, is given by Ohm's law:

$$R = \mu/I$$ (2)

Where μ is the potential difference (Voltage) and I is the current.

As resistivity and conductivity are inverse (i.e. $\sigma = 1/\rho$), these terms are used interchangeably.

Electrical resistivity surveys generally require a minimum of four electrodes: two current electrodes (A and B) that inject the current and two other electrodes (M and N) that record the resulting potential difference, μ. The potential difference is given by the following equation:

$$\mu = \frac{\rho I}{2\pi}\left[\frac{1}{AM} - \frac{1}{BM} - \frac{1}{AN} + \frac{1}{BN}\right]$$ (3)

Where AM, BM, AN and BN represent the distance between the electrode pairs respectively.

From here the apparent electrical resistivity can be calculated using:

$$\rho_a = \left[\frac{2\pi}{\left(\frac{1}{AM}\right) - \left(\frac{1}{BM}\right) - \left(\frac{1}{AN}\right) + \left(\frac{1}{BN}\right)}\right]\frac{\mu}{I}$$ (4)

$$= K\frac{\mu}{I}$$

Where K is a geometrical coefficient that is controlled by the arrangement of the four electrodes.

Resistivity data were collected on all three transects using ZZResistivity's FlashRES64 system. The FlashRES64 is a 61-channel, free configuration, multi-electrode, full-waveform electric resistivity system that includes a dedicated 2.5D inversion program (FlashRES64 manual, 2013).The system differs from the more traditional electric resistivity data collection techniques, as it does not limit itself to the standard ABMN electrode combinations (eg. Dipole-Dipole, Wenner and Schlumberger configurations) but uses nearly every possible combination of transmitter and receiver pairings (Zhe et al. 2007). 61-channels of data are collected in parallel for each dipole current pair; over 60,000 data points can be collected in under an hour (FlashRES64 manual, 2013). The field set up of the system can be seen in Figure 5. Data were collected using 1.5m electrode spacing, with each electrode being salted and watered, before running the acquisition (as configured here ~15000 data points were collected).The transmitted waveform was a square wave with a 6 second period; output voltage was limited to 250V. Transect 1 (Rocky Paddock) and Transect 2 (Chalkies) had an overlap of 14 electrodes between each spread. Data was collected for Transect 3 (Canham Rd) one month later and had an overlap of 11 electrodes. Data inversion was conducted using flash2res2dinv, a 2.5D resistivity inversion program (Bing and Greenhalgh 1999), producing smooth model 2D true resistivity depth sections.
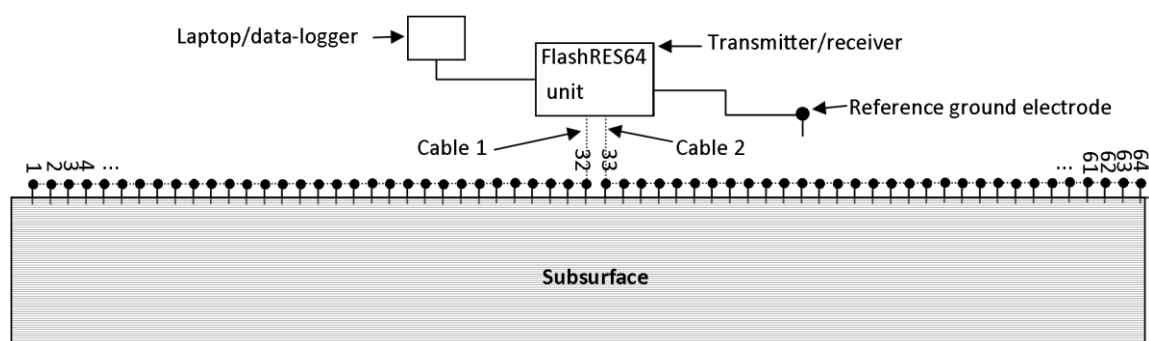
Figure 5: Schematic diagram of the field set-up for a surface survey using the FlashRES64 resistivity system (modified from FlashRES64 user manual, 2013). Dotted lines represent the electrode cables.

Frequency Domain Electromagnetics (FDEM) method

FDEM conductivity meters work by passing an alternating current at a desired frequency through the transmitting coil, generating a primary magnetic field H_p. This induces very small eddy currents in the earth (Mcneill 1980). These currents generate a secondary magnetic field H_s. The receiver coil then senses both the primary and secondary magnetic fields (Mcneill 1980).

The secondary magnetic field is generally a complicated function of the operating frequency, f, the intercoil spacing, s, and ground conductivity, σ (Mcneill 1980). In conditions where constraints meet the requirements of "operation at low induction numbers" the secondary magnetic field becomes a simple function of these variables (Mcneill 1980). The ratio between the primary and secondary magnetic field can then be simplified to:

$$\frac{H_s}{H_p} = \frac{i\omega\mu_o\sigma s^2}{4} \tag{5}$$

Where H_s is the secondary magnetic field at the receiver coil

H_p is the primary magnetic field at the receiver coil

ω: 2πf

f: frequency

μ_o: permeability of free space

σ: ground conductivity (S/m)

s: intercoil spacing (m)

$i = \sqrt{-1}$

The ratio between the secondary and primary magnetic field is now proportional to the terrain conductivity (Mcneill 1980). Given H_s/H_p the apparent conductivity shown by the instrument can be defined from equation (5) as:

$$\sigma_a = \frac{4}{\omega \mu_o S^2} \left(\frac{H_s}{H_p} \right) \qquad (6)$$

The DUALEM-421 is a frequency domain terrain conductivity meter, which calculates conductivity based on low induction number (LIN) approximation (Mcneill 1980). The transmitter is a horizontal loop, while receivers are both horizontal and vertical loops at three different spacings. This results in data being collected in both the horizontal co-planar (HCP) and perpendicular (PRP) modes. Three nominal separations are used: 1m, 2m and 4m respectively, resulting in 6 measurements being recorded at each location. Triantafilis et al. (2013) show that for the HCP receivers, the instrument is most sensitive from 0-1.5m (1m horizontal spacing), 0-3.0m (2m horizontal spacing) and 0-6m (4m horizontal spacing) respectively. Triantafilis et al. (2013) show that the PRP receivers are located at 1.1m, 2.1m and 4.1m, indicating the instrument is most sensitive at 0-0.5m (1.1m perpendicular spacing), 0-1m (2.1m perpendicular spacing) and 0-2m (4.1m perpendicular spacing) in this mode. Data were collected by connecting the DualEM-421 up to a Holland Scientific GeoSCOUT data logger (GLS-400) and differential GPS. Each transect was measured, with the unit carried at approximately 20-30cm above the ground surface. The data were inverted (J. Triantafilis pers. comm. 2013) using the EM4Soil software package (EMTOMO 2013). Em4Soil is a commercially available software package providing inversion algorithms for Geonics and DUALEM frequency domain electromagnetics instruments (EMTOMO 2013). A non-linear, 1-dimensional laterally constrained inversion process, also called a quasi-two-dimensional inversion (Q2D), described in Santos et al. (2010a) is used to process the DUALEM-421 conductivity data collected along the transects. The inversion algorithm consists of 1-D inversion with 2-D smoothness constraints between neighbouring 1-D inversions (Santos et al. 2010b). Inverted data was then contoured using Golden Software's Surfer8 program.

Ground Penetrating Radar (GPR) method

GPR is an electromagnetic reflection method with physical principles comparable to those that reflection seismic surveys are based upon (Blindow 2008). GPR produces images of the subsurface through the systems response to electrical discontinuities caused by the generation, propagation, transmission, reception, refraction and reflection of high frequency electromagnetic waves (Słowik 2012). Electromagnetic waves are reflected and diffracted when they contact a boundary between two mediums with different electrical properties (Blindow 2008). Subsurface lithologic boundaries are visible as reflections due to contrasts in the dielectric constant (Jol and Smith 1995). The reflectivity of layer boundaries and penetration depths are controlled by the petrophysical properties; electric permittivity ε and electric conductivity σ (Blindow 2008). The frequency of the transmitting antenna determines the depth and resolution of the survey, where generally the higher the frequency the higher the resolution but lower depth penetration (Neal 2004). Resolution of GPR antennas is approximately one quarter of the dominant wavelength. Increases in water content sees a reduction in propagation velocity, with increased clay content causing attenuation of GPR signal (Neal 2004).

GPR surveys use short electromagnetic pulses that are transmitted into the ground (Blindow 2008). When the electromagnetic wave contacts a layer boundary with different electrical properties, or a buried object, part of the energy is reflected or scattered. The direct and reflected amplitudes of the electric field strength **E** are recorded as a function of travel time (Blindow 2008). High pulse rates enable quasi-continuous measurements to be taken, allowing the transceiver to be moved smoothly along a profile at speeds of several kilometres per hour.

Under low loss conditions the phase velocity *v* of the radar waves can be calculated using:

$$v \cong \frac{1}{\sqrt{\mu\varepsilon}} \tag{7}$$

Where μ is magnetic permeability and ε is dielectric permeability.

Ground Penetrating Radar (GPR) fieldwork was conducted using MALA Geoscience's X3M Control unit. Four different frequency fixed separation shielded antenna (100, 250, 500 and 800 MHz) were tested. Data were collected for each antenna along all three of the transects. Location data were collected simultaneously using a differential GPS attached to the GPR unit. Each transect was walked twice. Data were processed using the ReflexW software package (D. Cremasco pers. comm. 2013).

Soil analysis method

Soil sampling was conducted concurrently with geophysical surveying to provide ground truthing for the geophysics. This consisted of drilling, using a rig-mounted hollow 60 mm percussion tube drill capable of extracting intact cores to 9 m. This method was used to provide soil samples most commonly at 20m intervals. There were some exceptions at Transect 2 based on time and access constraints. Samples were taken at regular depth intervals, with a portion placed into the chip tray and another sample bagged, weighed and labelled for further soil analysis. Changes in soil horizons were recorded along with sample hardness.

Further soil analysis was conducted in the laboratory. This included drying the samples in a 105°C oven until they displayed no further weight change. Dried samples were then weighed and moisture (weight%) was calculated from the difference in wet and dry weights. Dried samples were then passed through a 2mm sieve. This separated the samples into two fractions, each of which was weighed and bagged separately. EC 1:5 measurements

(Rayment and Higginson 1992) were made using 5 gram samples of the less than 2mm
fraction.

RESULTS AND COMPARISONS

Geophysical data was collected using GPR, resistivity and FDEM (DualEM) at all of three
transects. Resistivity and DualEM-421 data were inverted to produce 2-D depth sections for
the three transects, while GPR data were processed to produce reflection profiles suitable for
bedrock depth estimation where applicable. The 500MHz GPR data was selected for analysis.
Data have been separated into the three transects. DualEM and resistivity plots have been
displayed using log scales due to the large range of resistivity values observed. Moisture
content (weight %) and EC 1:5 were quantitatively analysed and compared with geophysical
data. Further soil data is available in Appendices B,C & D.

Transect 1: Rocky Paddock

The processed data are shown in Figure 6 and include a 2-D depth section generated from the
inversion of resistivity data (Figure 6a), a 2-D depth section generated from the inversion of
the DualEM-421 data (Figure 6b) and the processed 500MHz GPR data (Figure 6c). Figure
6a, 6b and 6c have been aligned based on the GPS positions and drill-hole locations. The 2-D
resistivity depth section (Figure 6a) was generated from the three spreads of resistivity data
collected at Rocky Paddock. Each of the spreads consists of approximately 10000-15000 data
points. The inverted data shows two sections of varying resistivity, with two distinct
conductors beneath DH11. Areas shown in white are below the indicated resistivity limit.
The DualEM depth section (Figure 6b) was generated from the inversion of approximately
1000 data points. The inverted data shows a three layer subsurface model (resistor, conductor,
resistor), with higher resistivity values in the first 100m. GPR profile is generated from

processed and filtered data (see appendix for data processing details). Signal is limited to the top metre at transect 1 using the 500MHz antenna.

The moisture (weight %) and EC 1:5 data collected for the drill-holes were analysed for correlation with the geophysical data sets. They were plotted as discrete drill-hole based depth sections along the profile, as shown in Figure 7. There is very little change in the EC 1:5 values as shown by Figure 7b, while moisture shows more variation as seen in Figure 7a. Drilling was conducted after geophysical surveying and included an extra drill-hole at 260m that geophysical surveying did not cover.
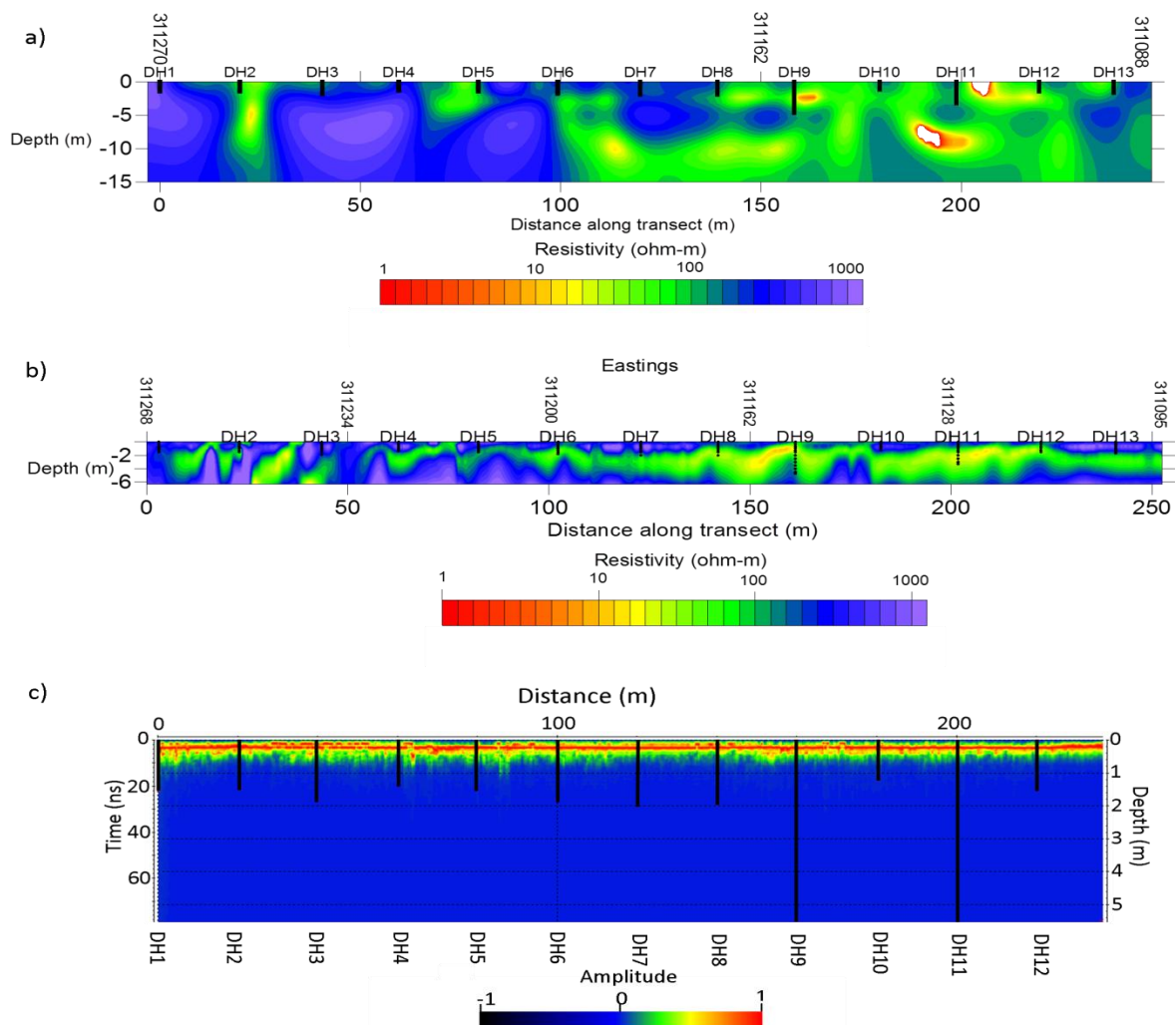
Figure 6: Geophysical models generated through the processing of data collected at Transect 1:Rocky Paddock. a) shows the 2-D depth section generated from the inversion of the resistivity data. b) shows the 2-D depth section generated from the inversion of the DualEM-421 data. c) shows the processed GPR data collected using the 500 MHz antenna. Drill-holes have been overlayed and labelled on a), b) and c).

a)

b)
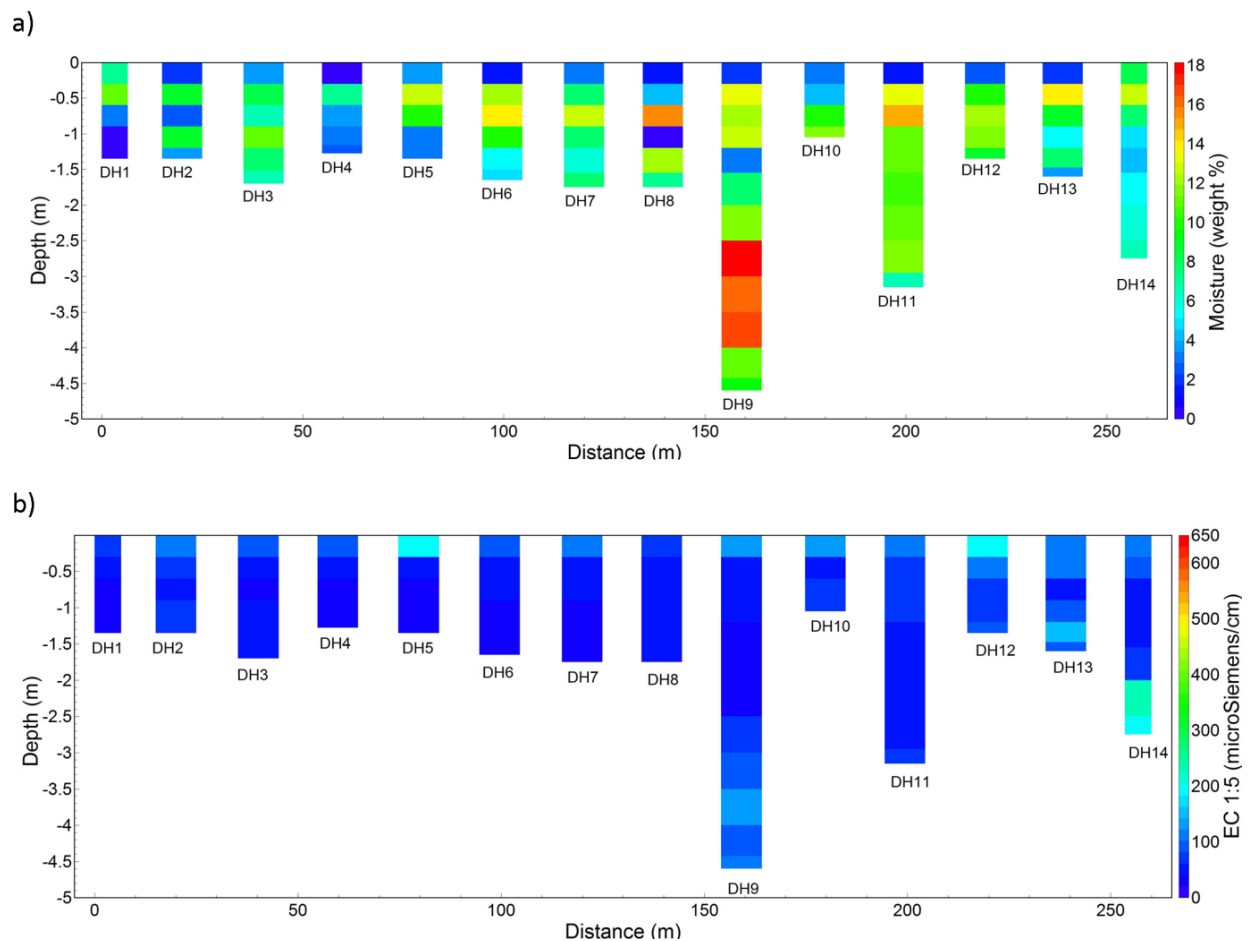
Figure 7: Transect 1drill-hole data generated from the soil analysis program. a) shows the moisture content (weight %) of the soil samples. b) shows the EC 1:5 values (microSiemens/m) measured for the <2mm fraction of the soil samples.

Transect 2: Chalkies

The processed geophysical data is shown in Figure 8 and includes a 2-D depth section generated from the inversion of resistivity data (Figure 8a), 2-D depth section generated from the inversion of the DualEM data (Figure 8b) and the processed 500MHz GPR data (Figure 8c). Figure 8a, 8b and 8c have been aligned using GPS coordinates and drill-hole positions. The 2-D resistivity depth section (Figure 8a) was generated from the three overlapping spreads of resistivity data collected at Rocky Paddock. Each of the spreads consists of approximately 10000-15000 data points. The inverted data shows a four layer subsurface

model (resistor, conductor, resistor, conductor), interrupted by a large resistor between DH7 and DH11. The DualEM depth section (Figure 8b) was generated from the inversion of approximately 3000 data points. The inverted DualEM data shows a three layer subsurface (resistor, conductor, resistor) interrupted by a large resistor between DH7 and DH11. GPR profile is generated from processed and filtered data (see appendix for data processing details). GPR data shows less than 1 metre depth penetration for the majority of Transect 2, with a zone of 1-2 metre depth penetration between DH8 and DH12.

The moisture (weight %) and EC 1:5 data collected for the drill-holes were analysed to see if there was a correlation with the geophysical data sets. They were plotted as discrete drill-hole based depth sections, and are shown in Figure 9.
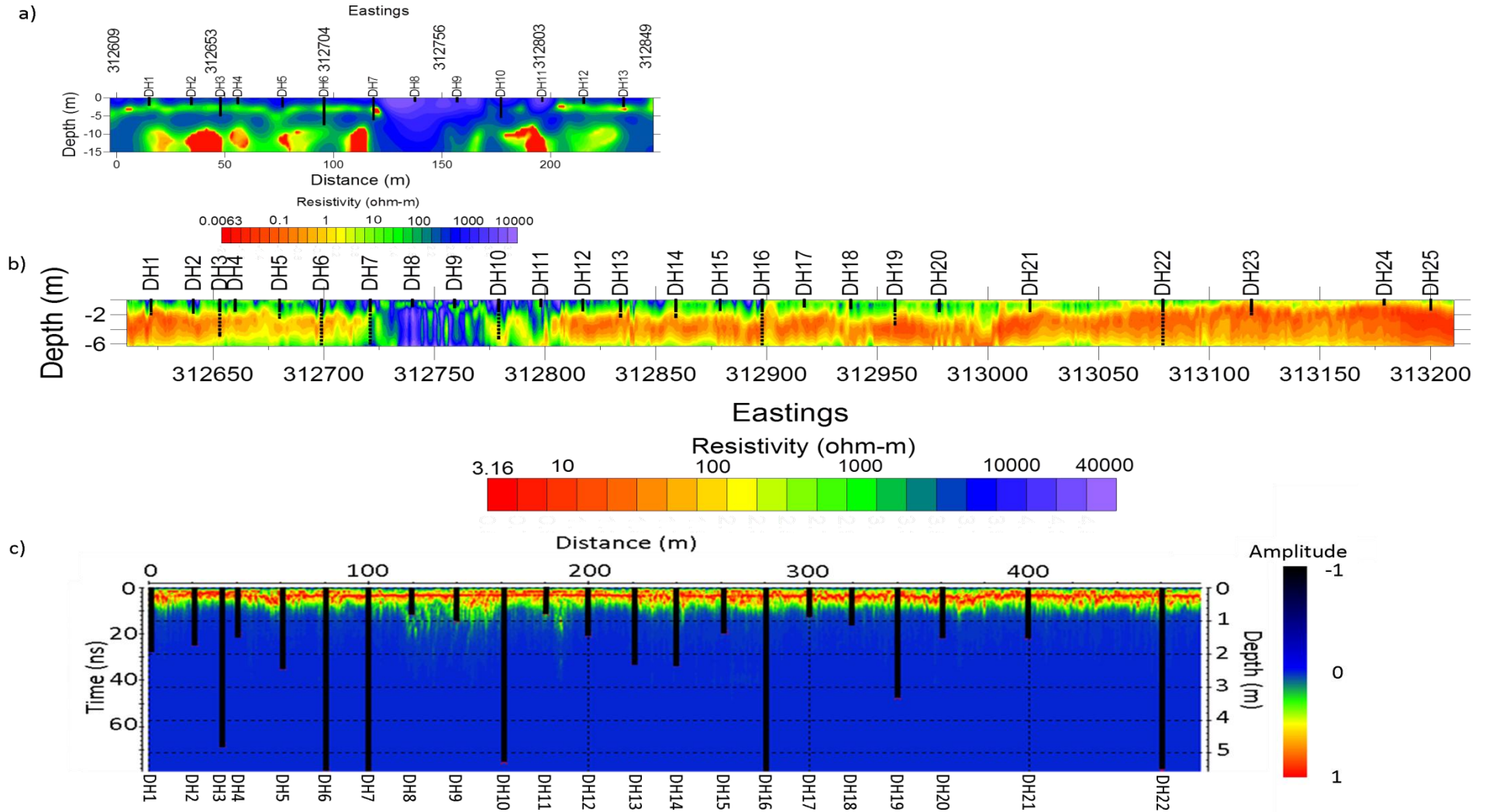
Figure 8: Geophysical models generated through the processing of data collected at Transect 2:Chalkies. a) shows the 2-D depth section generated from the inversion of the resistivity data. b) shows the 2-D depth section generated from the inversion of the DualEM-421 data. c) shows the processed GPR data collected using the 500 MHz antenna. Drill-holes have been overlayed and labelled on a), b) and c).
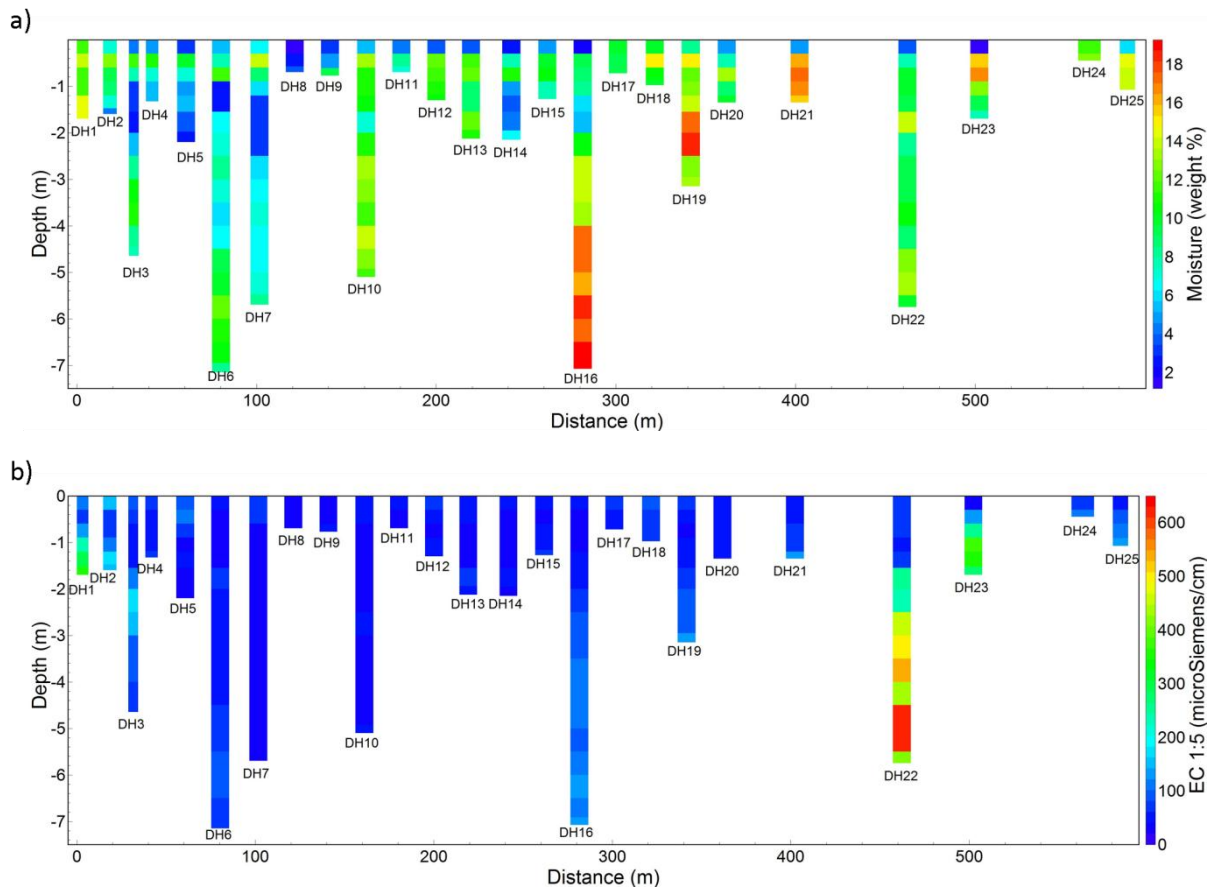
Figure 9: Transect 2 drill-hole data generated from the soil analysis program. a) shows the moisture content (weight %) of the soil samples. b) shows the EC 1:5 values (microSiemens/m) measured for the <2mm fraction of the soil samples. Drill-hole 1 is at 0m and drill-hole 25 is at 580m.

Transect 3: Canham Rd

The processed geophysical data are shown in Figure 10 and includes a 2-D depth section generated from four resistivity spreads stitched together (Figure 10a), 2-D depth section generated from the inversion of the DualEM data (Figure 10b) and the processed 500MHz GPR data (Figure 10c). Figures 5a, 5b and 5c have been aligned using GPS coordinates and drill-hole positions. The 2-D resistivity depth section (Figure 10a) was generated from the four spreads of resistivity data collected at Canham Rd. Resistivity data were collected one month after drilling and other geophysical data sets. Each of the spreads consists of approximately 10000-15000 data points. The inverted data (Figure

10a) shows two sections of varying resistivity; a resistive first 100m, followed by a more conductive region. The contact between the two merges is visible at 155m. The DualEM depth section (Figure 10b) was generated from the inversion of approximately 2000 data points. The inverted DualEM data shows a three layer subsurface (resistor, conductor, resistor), with a small zone of high resistivity at the start of the transect. GPR profile is generated from processed and filtered data (see appendix for data processing details). GPR signal is limited to the top metre.

The moisture (weight %) and EC 1:5 data collected for the drill-holes were analysed to see if there was a correlation with the geophysical data sets. They were plotted as discrete drill-holes along Transect 3 as shown in Figure 11. There is very little change in the EC 1:5 values as shown by Figure 11b, while moisture shows more variation as seen in Figure 11a. Drilling was conducted in the opposite direction to geophysical surveying. DualEM-421 data was collected for the entire 340m, however issues with the GPS signal due to vegetation cover resulted in unusable data from easting 314207 onwards. There is no processed geophysical data coverage of DH18.
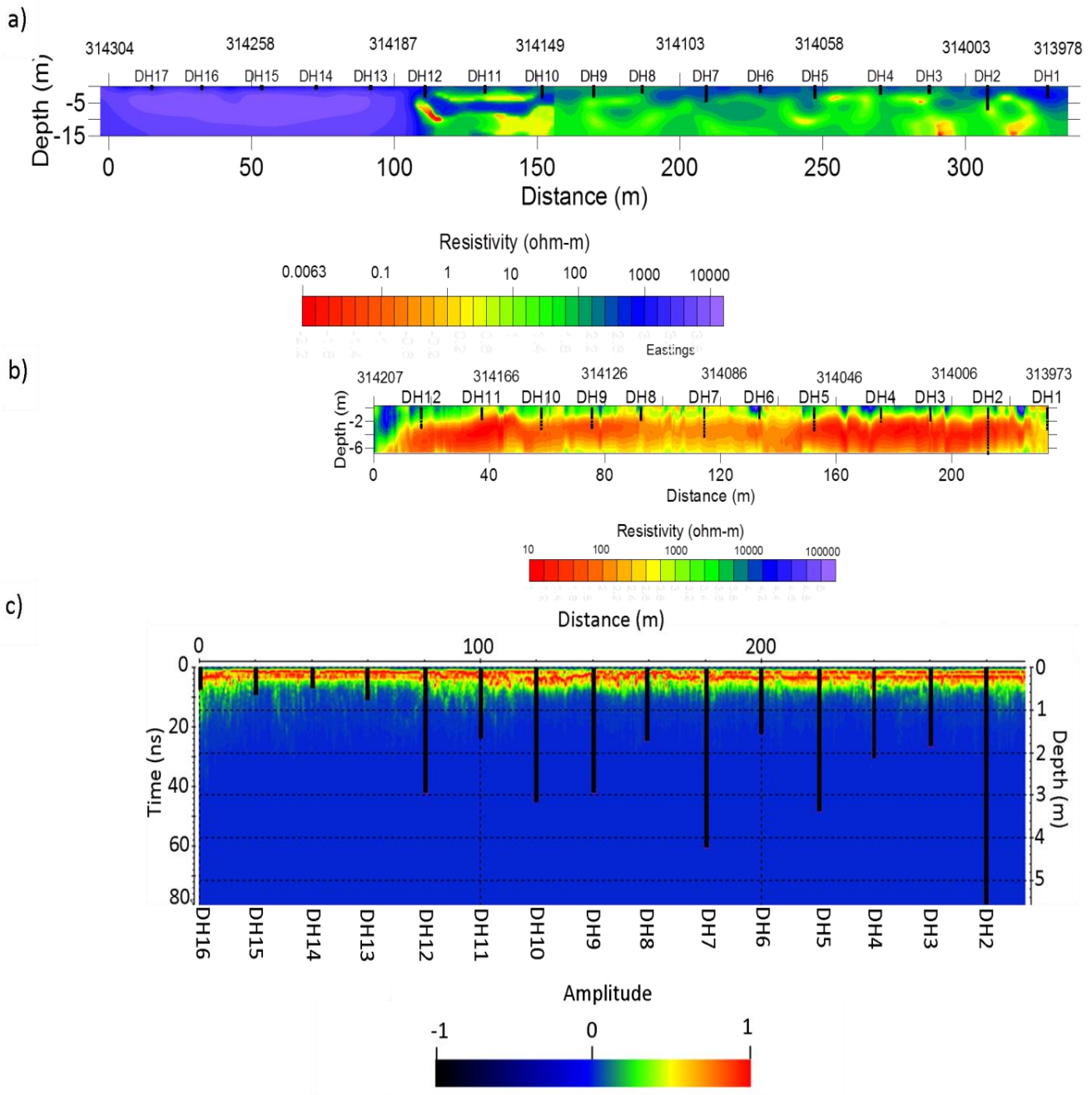
Figure 10: Geophysical models generated through the processing of data collected at Transect 3 (Canham Rd). a) shows the 2-D depth section generated from stitching two consecutive inversions of the resistivity data. b) shows the 2-D depth section generated from the inversion of the DualEM-421 data. c) shows the processed GPR data collected using the 500 MHz antenna. Drill-holes have been overlayed and labelled on a), b) and c).

a)

b)
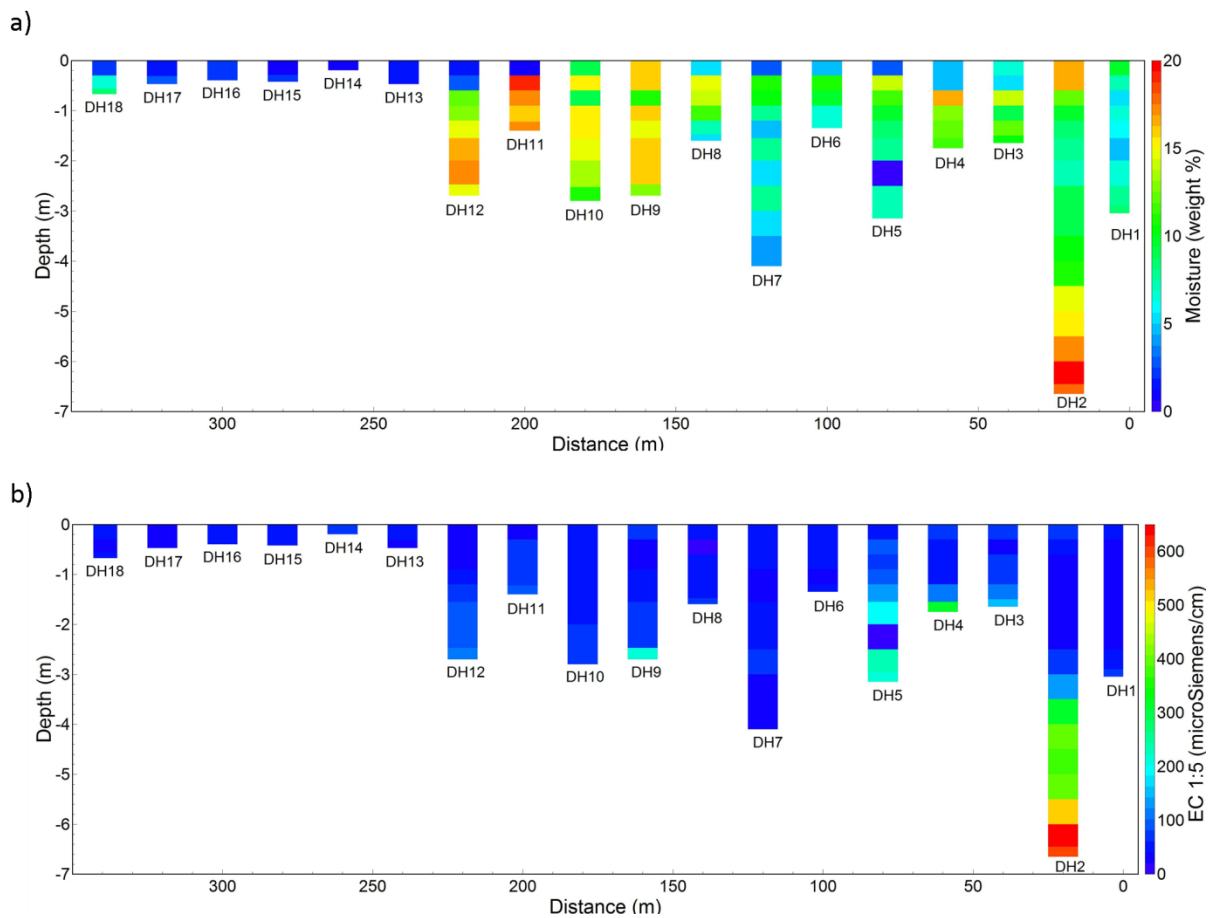
Figure 11: Transect 3 drill-hole soil data plots generated from the soil analysis program. a) shows the moisture content (weight %) of the soil samples. b) shows the EC 1:5 values (microSiemens/m) measured for the <2mm fraction of the soil samples. Drill-hole 1 is at 0m and drill-hole 18 is at 340m.

Transect 1: Rocky Paddock Comparisons

To improve comparison of data sets, Figure 12 presents the resistivity and DualEM data

sets plotted using the same scale and colour scale. When compared, the inverted 2-D

depth sections generated from the resistivity and DualEM data show similarities in the

overall trends observed at Transect 1. There are several differences in smaller scale

features. Both resistivity and DualEM show a trend of a more resistive subsurface for

the first 100-150m, before a shift to a relatively less resistive subsurface for the

remainder of Transect 1 (see Figure 12). There is correlation between the locations of

the least resistive "pods" seen in both plots near drill-holes 9 and 11. Differences between the inversions of the two techniques include resistivity indicating the presence of 3 large resistors in the first 100m, whereas the DualEM indicates a 3 layer model (resistor, conductor, resistor). DualEM (Figure 12b) has indicated a more resistive surface layer than is seen in the resistivity (Figure 12a). The resistivity inversion has produced a smoother model, while the DualEM inversion has produced more variation in the shapes of units. GPR data of Transect 1 (Figure 6c) showed almost no variation, with signal having been attenuated at depths less than a metre.
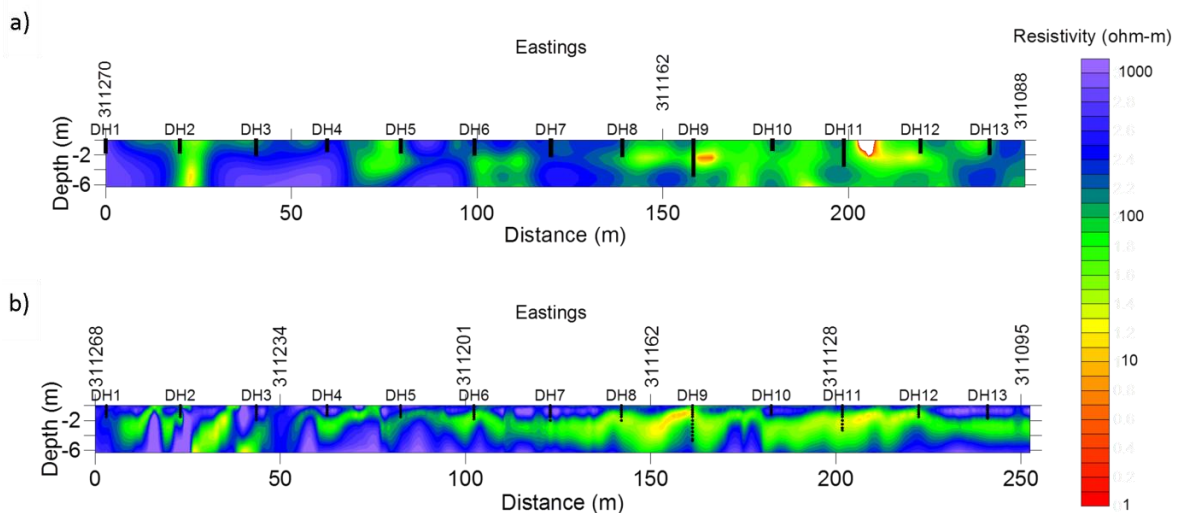
Figure 12: Inverted 2-D depth sections of (a) resistivity and (b) DualEM data collected over Transect 1. Plots use the same colour scale and depth parameters for direct comparisons between the two techniques. Drill-holes have been overlain to display known drill refusal depths.

Transect 2: Chalkies Comparisons

To improve comparison of data sets, Figure 13 presents the resistivity and DualEM data sets plotted using the same scale and colour scale. There are strong similarities between the inverted 2-D depth sections of the resistivity and DualEM data. These similarities are best represented when plotted using the same colour scale and depth limits, as shown in Figure 13. Both models show a resistive band along the top 1-2 metres. The resistivity values of this layer are higher in the DualEM data compared to the resistivity.

This layer is underlain by a less resistive layer (100-200 ohm-m) shown on both plots. This layer is approximately 4-5 metres thick. This layer displays a centre of less resistive (1-10 ohm-m) material. The layering seen on both the resistivity and DualEM plots is interrupted by a large resistive unit that extends from DH 7 to DH 10. This unit displays values of over 10000 ohm-m at its centre. The depths to drill refusal are much shallower in this unit. This supports the geophysics data which suggests very shallow bedrock in this location. There is also a notable increase in the depth of signal of the GPR data (Figure 8c) that coincides with this resistive unit. Examination of chip-tray contents in this resistive zone shows the presence of coarser, higher sand content regolith underlain by a quartzite/quartz sandstone bedrock. This is very different to the chip tray samples that occur on either side of this resistive zone, which display fine grained, micaceous sediments and clays.
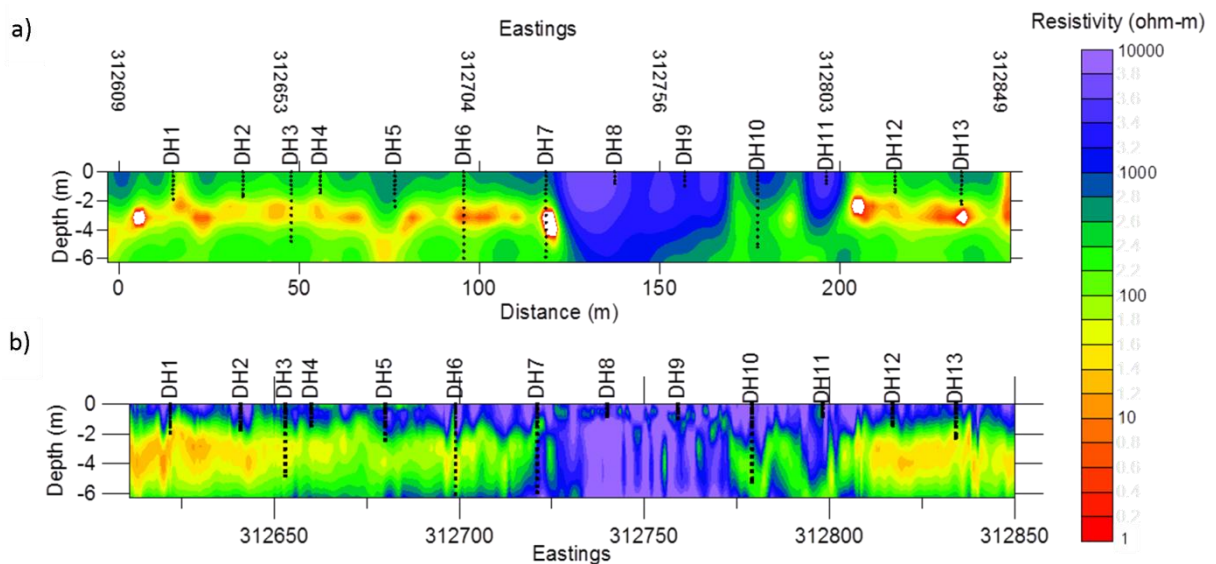
Figure 13: Inverted 2-D depth sections of (a) resistivity and (b) DualEM data collected over Transect 2. Plots use the same colour scale and depth parameters for direct comparisons between the two techniques. Drill-holes have been overlain to display known drill refusal depths.

Transect 3: Canham Rd Comparisons

To improve comparison of data sets, Figure 14 presents the resistivity and DualEM data sets plotted using the same scale and colour scale. Resistivity and DualEM-421 show similarities in the models generated of the subsurface. DualEM data shown in Figure 14b is shorter than the resistivity shown in Figure 14a due to problems with the GPS during data collection. This data had to be removed prior to inversion. The inverted resistivity depth section (Figure 14a) shows a large, relatively homogenous resistive unit (>1000 ohm-m) for the first 100m. The western edge of this unit coincides with a unit seen at the start of the DualEM plot. Outside of this resistor the plots appear to display a 2-3 layer subsurface model. The resistivity appears to be higher resolution, with smoother layer boundaries, however the overall trends appear to strongly correlate. Both plots show a distinct band of 10-100 ohm-m material between drill-hole 12 and drill-hole 8. This band appears to increase in resistivity to 100-200 ohm-m between drill-hole 8 and drill-hole 5. It then decreases in resistivity again to 10-100 ohm-m (with small pods of less resistive material) until displaying a small 1000 ohm-m resistive unit at drill-hole 1. The GPR data (Figure 10c) shows a minor decrease in depth penetration and signal strength in the resistive unit seen in the first 100 metres. The depth at which signal begins to rapidly attenuate in this region correlates strongly with the depth of drill refusal.
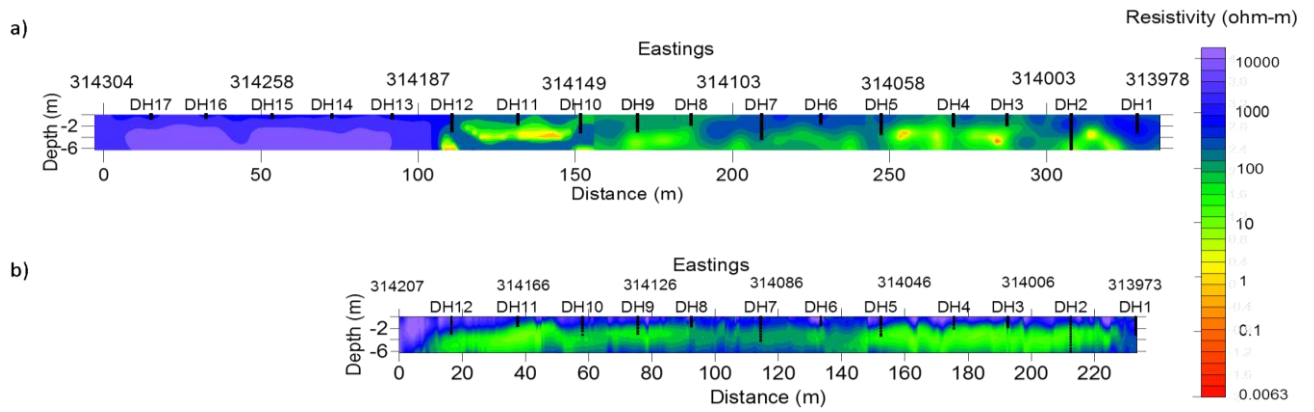
Figure 14: Inverted 2-D depth sections of (a) resistivity and (b) DualEM data collected over Transect 3. Plots use the same colour scale and depth parameters for direct comparisons between the two techniques. Drill-holes have been overlain to display known drill refusal depths.

DISCUSSION

The effectiveness of different geophysical techniques to determine the depth to bedrock in the Mount Crawford region requires careful consideration. Differences in the observed resistivity models generated by the resistivity and Dual-EM may be related to the use of different inversion algorithms. The majority of the variation is, however, more likely related to the nature of the geophysical techniques. Resistivity is a galvanic technique, which depends on direct ground contact to transmit and receive signal, while the Dual-EM is an inductive technique and GPR is an electromagnetic pulse reflection technique. Each of these systems has differences in the resolution, depth of investigation and responses to varying lithologies based on the principles behind them.

Direct comparisons of the techniques over the same transects demonstrate the differences in the observed system responses. With drill-refusal depth known at intervals (most commonly 20m) along the transects the geophysics can be compared to quantitative data collected from the drilling program. Interestingly, along the three transects bedrock is identified as a conductor, in other settings bedrock most commonly appears in resistivity and EM surveys as relatively resistive compared to overlying regolith (Chaplot et al. 2010, Shafique et al. 2011, De Vita et al. 2006). The success of each technique needs to be analysed based on its own merits at each individual transect due to the significant differences in the geophysical responses. Bedrock has been interpreted using drill refusal, inverted DualEM-421 2-D depth sections and inverted resistivity 2-D depth sections. The qualitative comparison of the interpreted bedrock horizons for the three transects is shown in Figure 15.
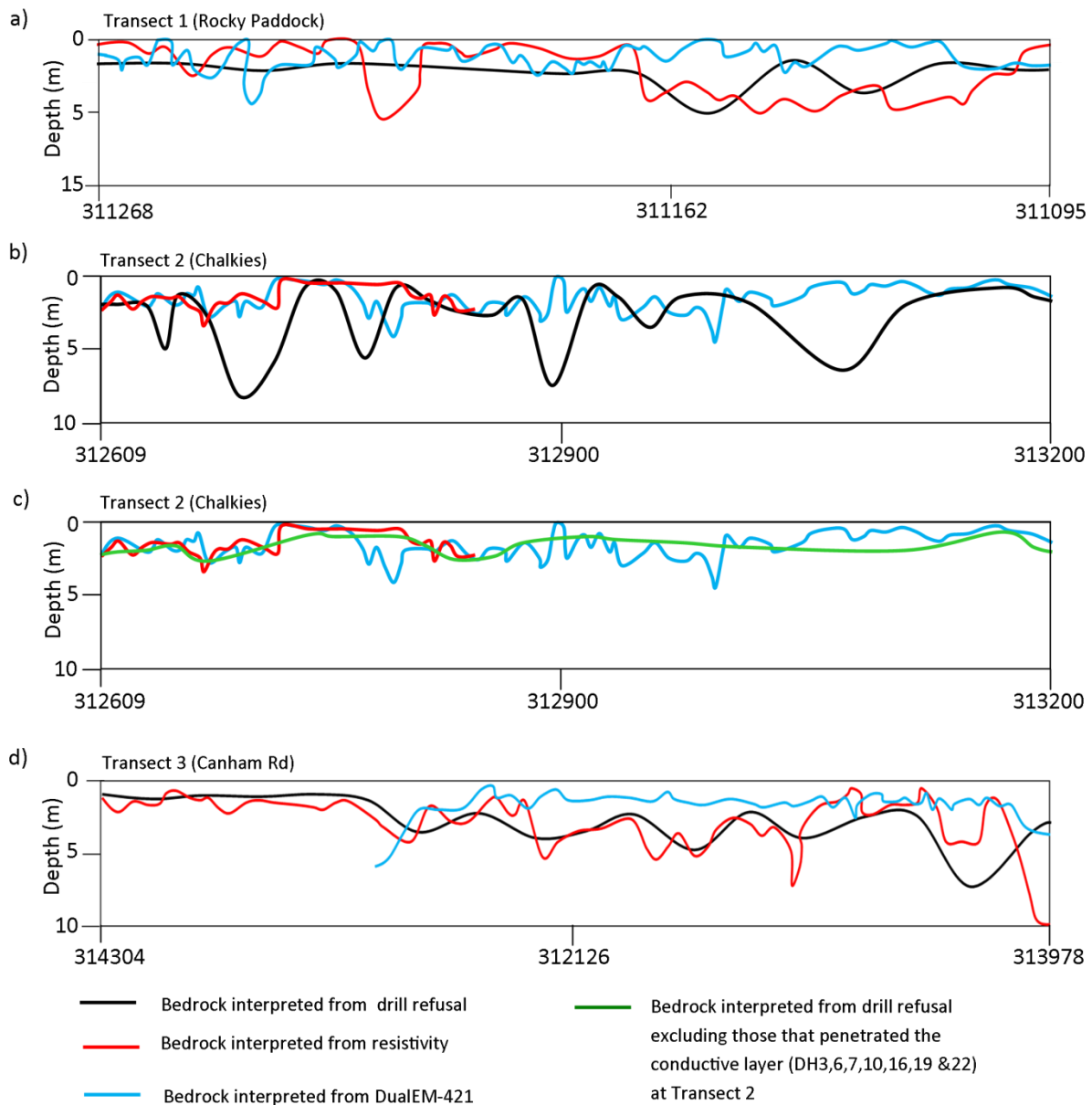
Figure 15: Interpretation of bedrock using known drill refusal depths as well as the interpreted response of bedrock in the inverted resistivity and DualEM-421 depth sections. a) shows the interpreted bedrock of Transect 1: Rocky Paddock. b) shows the interpreted bedrock of Transect 2: Chalkies. c) shows the interpreted bedrock from drill refusal at Transect 2: Chalkies if the drill-holes that penetrate the top conductive layer (DH 3,6,7,10, 16 and 22) are removed. d) shows the interpreted bedrock of Transect 3: Canham Rd.

Transect 1: Rocky Paddock

Using geophysics to estimate depth to bedrock at Transect 1 (Figure 6) was challenging because the resistivity, DualEM and GPR all produce different responses to the subsurface. These differences, coupled with a lithological change along the transect meant there was no characteristic bedrock response displayed by the three analysed techniques. The processed GPR (Figure 6c) shows almost no change along Transect 1, with signal attenuated between 0.5-1m depths. Attenuation is most commonly associated with the presence of clays and/or wet sediments (De Benedetto et al. 2010). Based on this, it is likely that the observed attenuation of signal is related to the presence of conductive sediments. The GPR response displays no evidence of a change in lithology as seen in the resistivity, and to a lesser extent the DualEM-421. The inverted resistivity and DualEM-421 depth sections indicate a predominantly resistive subsurface for the first 100-150 metres. GPR should receive good signal in this resistive region. With relatively low EC 1:5 values, low moisture values and low clay content it is likely that it is the mineralogy of the sediments that causes GPR attenuation. For example, Josh et al. (2011) showed that an iron coating on quartz grains can cause rapid attenuation of GPR signal even in seemingly favourable environments. His study showed that although the study area consisted of 90% quartz, iron concentrations of just 0.4% were enough to cause rapid attenuation. There is no indication of iron coating on the samples in this area, nevertheless it is likely that there is a similar mechanism that is attenuating the signal in this area. It appears that GPR is unsuitable for bedrock depth estimation along this transect.

The inverted 2-D resistivity model (Figure 6a) for this transect contains a shift in relative resistivity, separating the resistive first 100-150m from the rest of the transect. The first half is dominated by large resistive bodies. These resistive bodies are interpreted to be gneissic bedrock buried beneath approximately 1-2m regolith, as seen in the chip tray samples for these drill-holes. Depths to the top of the resistive units, as interpreted from the resistivity inversion correlates well with known drill refusal depths in this resistive region. It is difficult to determine a specific resistivity value that represents the bedrock/regolith boundary. The zone of lower resistivity is interpreted to represent a shift to weathered schistose rocks and micaceous sediments, as these are present in the chip trays from the drill-holes in this zone. The less resistive region, seen between DH 9 and DH13, shows bedrock characteristic features becoming less distinguishable. This results in resistivity proving less effective at determining bedrock depth in this zone. Figure 15a shows that the resistivity provided a much more variable interpretation of bedrock than the smooth interpretation generated from drill refusal. The correlation appears overall to be weak, suggesting that resistivity was not suitable for accurately determining bedrock depth in this location. This correlation has been affected by the presence of the relatively less conductive regions that separate the large resistive bodies, seen below DH2 and DH5. Drilling in this region indicates no change in refusal depth, suggesting there is no major change in bedrock depth.

Depth to bedrock was more difficult to determine from the DualEM (Figure 6b) data because the model generated had considerable variation in features and did not smoothly define layer boundaries. The DualEM data displayed a similar response to the resistivity, indicating a more resistive first 100-150m, followed by a more conductive

subsurface. The DualEM, however, displayed poor resolution of the three large resistors shown in the first 100m of the inverted resistivity plot (Figure 6). The DualEM appeared to be imaging a more continuous band of lower resistivity material than the inverted resistivity depth section. Depth to bedrock was interpreted in the DualEM-421 data to be represented by the conductive band that extended across the transect. When plotted against the interpreted bedrock depth using drill refusal (Figure 15A) it shows a weak correlation for the first 150m, before indicating a shallowing of bedrock, where in fact bedrock deepened. A smoothing function may help to achieve a more realistic bedrock prediction.

Transect 2: Chalkies

Of the three transects surveyed, Chalkies showed the most consistent results between the three geophysical techniques and drill refusal depths (Figure 8). The inverted resistivity and DualEM depth sections showed strong correlation in subsurface features and depths. While the GPR signal was largely attenuated between 0.5-0.75m below the surface there was an increase in signal depth in the region that both the resistivity and DualEM-421 showed as a large resistive body extending to the surface. In this resistive unit the GPR signal shows a strong correlation with the depth of drill refusal. This suggests that in suitably resistive conditions the GPR has the potential to accurately delineate the regolith-bedrock boundary by showing a series of relatively strong reflections.

Both the resistivity and the DualEM-421 showed resistive material dominating the top 1-2m, potentially caused by lower moisture levels and weathered alluvium. This is underlain by a 2-3 metre thick conductive band, which appears to be a weathered

saprolitic layer of illitic (micaceous) dominated mineralogy. Analysis of the chip trays shows an increase in density and a change in colour to a whitish-green colour. There is a slight increase in the moisture content and EC 1:5 values as you move into this horizon (Figure 9a and b), however the increase is minimal. This small increase in moisture and EC 1:5 is unlikely to cause the reduction in resistivity values observed in this layer. It is more likely to be a result of an increase in clay content or a mineralogical change in this zone. Beneath this is a layer of higher resistivity material that may represent a less weathered saprolite, or even hard bedrock. This layer showed an increase in moisture values (Figure 9a) measured in the soil sampling program and a more defined rock fabric in the chip trays. There is a slight increase in the EC1:5 content (Figure 9b). To generate the higher resistivity values seen in this layer there is likely to be less connected pore space or a change in mineralogy. The final layer occurred deeper than the maximum depth of the deepest drill-hole and is most likely a highly saline body of water, with "pods" of more saline water accumulating in available pore spaces. There appears to be a pathway for fluids to connect to this conductive layer below DH 5, which also sees a dip in the upper conductive band. This may be a result of fracturing.

Both the inverted resistivity and DualEM depth sections (Figure 8 a & b) show a correlation between the drill refusal depths and the top of the shallow conductive layer. There are, however, several drill-holes (DH3, 6 & 7 in the resistivity and DH3, 6, 7, 10, 16, 19 & 22 in the DualEM) which penetrate through this layer, continuing to greater depths. The inconsistency of the refusal depths reduces the accuracy with which the depth to bedrock can be interpreted using the resistivity and DualEM. There is, however, evidence suggesting that both resistivity and DualEM were overall effective

tools for predicting the depth to bedrock (Figure 15b). The deeper drill refusals, although only occurring infrequently, appear to reduce the qualitative correlation between the geophysics and drill refusal based bedrock interpretation. Of the 13 drill-holes sampled in the area that resistivity data were collected, 7 of them terminated at the top of the uppermost conductive layer (±50cm) in Figure 8b. A further two drill-holes terminated at shallow depths in the resistive quartzite/quartz-sandstone unit. The DualEM showed that of the 25 drill-holes taken at Transect 2, 15 of these terminated at the top of the conductive layer(± 50cm), with a further 2 terminating at shallow depths in the resistive quartzite/quartz-sandstone unit. It is worth noting that the drill-holes which penetrated through the conductive layer may be reflecting localised conditions that the geophysics is not able to resolve and in fact may indicate the highly variable nature of saprolitic bedrock and the influence that the degree of weathering has on the depth of penetration of a push tube percussion drill. When the deeper drill-holes are removed from the drill-refusal interpretation of bedrock (Figure 15c) there is a strong correlation between the interpreted bedrock depths of the resistivity and DualEM-421 inversions to the known drill refusal depths.

Transect 3: Canham Rd

Determining depth to bedrock along Transect 3 largely relies on the use of resistivity and DualEM (Figure 10a & b). The GPR (Figure 10c) appears to show a series of reflections that correlate with the depth of refusal of DH13, 14, 15 and 16 which are found in a zone identified as resistive by the DualEM and resistivity depth sections. Signal appears to be rapidly attenuated at the depth of drill refusal. This suggests that the depth of drill refusal may correlate with a unit that causes attenuation of GPR signal.

Analysing the chip trays for this zone reveals that this resistor is mostly associated with heavily weathered, ferruginised sediments that are underlain by a silicified, ferruginised layer of calcrete. This is underlain by deep residual, highly weathered quartzite, with kaolinite present. Previous studies have revealed that calcrete can be poorly suited to GPR as it causes rapid attenuation of the signal (Daniels and Engineers 2004). There is also the potential for the ferruginous material to cause GPR signal attenuation by reducing the dielectric permittivity of the subsurface (Josh et al. 2011). The remainder of the transect sees attenuation of the GPR signal at depths much shallower than drill refusal, making it unsuitable for bedrock depth estimation.

Resistivity provides a moderately effective tool for determining bedrock depth on Transect 3. Similarly to what was seen in the large resistor at Transect 2, the first 100m of the resistivity survey shows a large resistor correlating with shallow drill refusal. Once the transect shifts to a less resistive subsurface a similar trend to Chalkies is again noticed, with drill refusal correlating with the top of less resistive material. This is supported by the DualEM-421 data, which although incomplete in total transect coverage, shows strong similarities to the resistivity model. Having two techniques both indicating the termination of drill-holes near the surface of a layer of lower resistivity, relative to the overlying regolith, increases the confidence in the abilities of the geophysical systems to correctly measure the subsurface resistivity/conductivity of the region. With two techniques producing similar inversion models, this supports the theory that either the underlying bedrock in the Mt Crawford region is anomalously conductive compared to the overlying regolith or that the push-tube percussion drill was unable to penetrate through conductive saprolite/dense clay horizons .

Figure 15d shows a qualitative correlation between the interpreted bedrock horizon generated from the inverted resistivity data and the drill-refusal defined bedrock horizon. There are some locations, particularly towards the end of Transect 3, where the correlation is weaker. This may be because bedrock interpreted from drill-refusals is based on 1 sample every 20m, whereas the geophysical techniques attempts to model the entire transect. Bedrock interpreted from the DualEM inversion shows a weaker correlation to the drill-refusal interpreted bedrock. The DualEM consistently interprets bedrock as being shallower than the known depths of drill refusal.

CONCLUSIONS

Establishing a method for characterising the depth to bedrock using geophysics has the potential to reduce the costs of future studies by reducing the reliance on drilling. This study qualitatively compared three geophysical techniques along three transects to understand environments in which they could be applied to determine depth to bedrock. Geophysical data was compared to drill-hole data that was collected for quantitative analysis. The geophysical responses differed at each of the transects and appeared to show a weak correlation to the moisture and EC1:5 data. The major findings of the study were the correlation of conductive layers in the inverted resistivity and DualEM depth sections with drill-refusal depth. This correlation was most evident at Transect 2 and to a lesser extent transect 3, where bedrock (or its weathered counterpart) appear to be anomalously conductive relative to overlying regolith. The study also indicated that GPR is largely unsuitable in the complex weathered landscapes of the Mount Crawford region, where signal is rapidly attenuated.

Problems included the variation in the depth of drill-refusal, which most commonly terminates at moderately weathered bedrock, as well as the rapid attenuation of GPR data. Without a drilling program that penetrates hard bedrock it is difficult to say with certainty where the hard bedrock boundary is. Further work needs to be conducted into understanding the mineralogy of the soils to help understand why GPR signal rapidly attenuated. This should include X-ray fluorescence (XRF) which will reveal the elemental composition of the regolith. Implementing different geophysical techniques, such as reflection seismic may prove to be more effective than those tested in this study. In conclusion, when choosing which technique is most suitable for future surveys it is important to consider your requirements, available time and most importantly the environment in which the study will be conducted. The GPR was largely ineffective due to signal attenuation at depths most commonly less than one metre. There was, however, evidence to suggest in suitably resistive soils that it can be effective and data can be rapidly collected. The DualEM-421 provides a fast data collection method that shows strong similarities to the resistivity data. The resolution of the data can be restricting at accurately defining horizons. The resistivity was the most time consuming technique, however it provided the strongest correlations to the drill-hole data.

ACKNOWLEDGMENTS

REFERENCES

BADMUS B. S., *et al.* 2012 3D electrical resistivity tomography survey for the basement of the Abeokuta terrain of Southwestern Nigeria, *Journal of the Geological Society of India,* vol. 80, no. 6, pp. 845-854.

BING Z. & GREENHALGH 1999 Explicit expressions and numerical calculations for the Fréchet and second derivatives in 2.5D Helmholtz equation inversion, *Geophysical Prospecting,* vol. 47, no. 4, pp. 443-468.

BLINDOW N. 2008 Groundwater Geophysics: A Tool for Hydrogeology. (2nd Edition edition). Springer, Berlin, Germany.

BRUS D. J., *et al.* 1992 The use of electromagnetic measurements of apparent soil electrical conductivity to predict the boulder clay depth, *Geoderma,* vol. 55, no. 1–2, pp. 79-93.

CHAPLOT V., *et al.* 2010 Digital mapping of A-horizon thickness using the correlation between various soil properties and soil apparent electrical resistivity, *Geoderma,* vol. 157, no. 3–4, pp. 154-164.

DANIELS D. J. & ENGINEERS I. O. E. 2004 Ground Penetrating Radar, 2nd Edition. Institution of Engineering and Technology.

DE BENEDETTO D., *et al.* 2010 Spatial relationship between clay content and geophysical data, *Clay Minerals,* vol. 45, no. 2, pp. 197-207.

DE VITA P., AGRELLO D. & AMBROSINO F. 2006 Landslide susceptibility assessment in ash-fall pyroclastic deposits surrounding Mount Somma-Vesuvius: Application of geophysical surveys for soil thickness mapping, *Journal of Applied Geophysics,* vol. 59, no. 2, pp. 126-139.

EMTOMO 2013 EMTOMO.

FRIEDMAN S. P. 2005 Soil properties influencing apparent electrical conductivity: a review, *Computers and Electronics in Agriculture,* vol. 46, no. 1–3, pp. 45-70.

HSU H.-L., *et al.* 2010 Bedrock detection using 2D electrical resistivity imaging along the Peikang River, central Taiwan, *Geomorphology,* vol. 114, no. 3, pp. 406-414.

JOL H. M. & SMITH D. G. 1995 Ground penetrating radar surveys of peatlands for oilfield pipelines in Canada, *Journal of Applied Geophysics,* vol. 34, no. 2, pp. 109-123.

JOSH M., *et al.* 2011 Impact of grain-coating iron minerals on dielectric response of quartz sand and implications for ground-penetrating radar, *Geophysics,* vol. 76, no. 5, pp. J27-J34.

LINDSAY J. M. & ALLEY N. F. 1995 Myponga and Hindmarsh Tiers Basins. In DREXEL J. F. & PREISS W. V. eds. The geology of South Australia, Vol. 2, The Phanerozoic. Geological Survey of South Australia. Bulletin 54. pp. 199-201.

MCGOWRAN B. 1989 The later Eocene transgressions in southern Australia, *Alcheringa: An Australasian Journal of Palaeontology,* vol. 13, no. 1, pp. 45-68.

MCNEILL J. D. 1980 *Electromagnetic Terrain Conductivity Measurement at Low Induction Numbers*, *Geonics Limited, Technical Note TN 6. Geonics Ltd, Mississauga, Ontario, Canada.*

NEAL A. 2004 Ground-penetrating radar and its use in sedimentology: principles, problems and progress, *Earth-Science Reviews,* vol. 66, no. 3–4, pp. 261-330.

PAILLET Y., CASSAGNE N. & BRUN J.-J. 2010 Monitoring forest soil properties with electrical resistivity, *Biology and Fertility of Soils,* vol. 46, no. 5, pp. 451-460.

PREISS W. V.*, et al.* 2008 Age and tectonic significance of the Mount Crawford Granite Gneiss and a related intrusive in the Oakbank Inlier, Mount Lofty Ranges, *MESA,* vol. 49, pp. 38-49.

RAYMENT G. E. & HIGGINSON F. R. 1992 Australian Laboratory Handbook of Soil and Water Chemical Methods*.* Inkata Press.

SAMOUËLIAN A.*, et al.* 2005 Electrical resistivity survey in soil science: a review, *Soil and Tillage Research,* vol. 83, no. 2, pp. 173-193.

SANTOS F. A. M.*, et al.* 2010a Inversion of Multiconfiguration Electromagnetic (DUALEM-421) Profiling Data Using a One-Dimensional Laterally Constrained Algorithm, *Vadose Zone Journal,* vol. 9, no. 1, pp. 117-125.

SANTOS F. A. M.*, et al.* 2010b Inversion of Conductivity Profiles from EM Using Full Solution and a 1-D Laterally Constrained Algorithm, *Journal of Environmental & Engineering Geophysics,* vol. 15, no. 3, pp. 163-174.

SENECHAL P., PERROUD H. & GARAMBOIS S. 2000 Geometrical and physical parameter comparison between GPR data and other geophysical data, pp. 618-623.

SHAFIQUE M., DER MEIJDE M. V. & ROSSITER D. G. 2011 Geophysical and remote sensing-based approach to model regolith thickness in a data-sparse environment, *CATENA,* vol. 87, no. 1, pp. 11-19.

SŁOWIK M. 2012 Influence of measurement conditions on depth range and resolution of GPR images: The example of lowland valley alluvial fill (the Obra River, Poland), *Journal of Applied Geophysics,* vol. 85, no. 0, pp. 1-14.

SUDDUTH K. A.*, et al.* 1995 Electromagnetic induction sensing as an indicator of productivity on claypan soils. In PROBERT P. G., RUST R. I. H. & LARSON W. E. eds. Proceedings of the Second International Conference on Site Specific Management for Agricultural Systems*.* pp. 671-681. Minneapolis, MN, USA.

TOKAREV V. 2005 Neotectonics of the Mount Lofty Ranges (South Australia). Faculty of Science*.* pp. 272. Adelaide: University of Adelaide.

TRIANTAFILIS J., HUCKEL A. I. & ODEH I. O. A. 2001 Comparison of Statistical Prediction Methods for Estimating Field-Scale Clay Content Using Different Combinations of Ancillary Variables, *Soil Science,* vol. 166, no. 6, pp. 415-427.

TRIANTAFILIS J. & LESCH S. M. 2005 Mapping clay content variation using electromagnetic induction techniques, *Computers and Electronics in Agriculture,* vol. 46, no. 1–3, pp. 203-237.

TRIANTAFILIS J., TERHUNE IV C. H. & MONTEIRO SANTOS F. A. 2013 An inversion approach to generate electromagnetic conductivity images from signal data, *Environmental Modelling & Software,* vol. 43, no. 0, pp. 88-95.

WILFORD J. & THOMAS M. 2012 modelling soil-regolith thickness in complex weathered landscapes of the central Mt Lofty Ranges, South Australia. In MINASNY B., MALONE B. P. & MCBRATNEY A. B. eds. Digital Soil Assessments and Beyond*.* pp. 69-75. Sydney, Australia: Taylor and Francis Group.

WILLIAMS B. G. & HOEY D. 1987 The Use of Electromagnetic Induction to Detect the Spatial Variability of the Salt and Clay Contents of Soils, *Aust. J. Soil Res,* vol. 25, pp. 21-28.

ZHE J., GREENHALGH S. & MARESCOT L. 2007 Multichannel, full waveform and flexible electrode combination resistivity-imaging system, *Geophysics,* vol. 72, no. 2, pp. F57-F64.

APPENDIX A: DETAILED METHODOLOGY

Data Collection

<u>Resistivity</u>
1. Transects were pre-surveyed, and electrodes were placed at 1.5m intervals.
2. Electrodes were hammered into the ground, salted and watered (approx 100-200mL per electrode).
3. Transmitter/receiver cables were connected to the electrodes, using spring clips.
4. Earthing electrode was hammered in, salted and watered at array centre.
5. The system was connected to the cables, laptop and power source (12v battery).
6. The Program FlashRES6 was turned on.
7. Electrodes were tested by program.
8. Parameters were set with 1.5 m electrode spacing, 3 second sample interval, quick survey (15000 data points) and at 250 volts.
9. Survey was run and data saved onto the computer.
10. Differential GPS data were collected at electrodes 1, 8, 16, 24, 32, 40, 48, 56 and 64.
11. Each Spread overlapped the previous spread by 14 electrodes for Rocky Paddock and Chalkies, and 11 electrodes at Canham Rd (which was collected at a later date).

<u>DUALEM-421:</u>
1. Connect Differential GPS to DUALEM-421.
2. Connect DUALEM-421 and GPS to Holland Scientific GeoSCOUT data logger (GLS-400)
3. The DUALEM-421 was held approximately 30cm above the ground by 2 people at a time, with a third person carrying the data-logger and a NovaTel SMARTV1 antenna for georeferencing.
4. The transects were then walked a minimum of 2 times, following as close to the line of drill-holes as possible.
5. Data were downloaded from GeoSCOUT data logger a field laptop for later processing.

<u>Ground Penetrating Radar</u>
1. Connect the antenna (100, 250, 500 or 800 MHz) to the GPR system.
2. Attach differential GPS to the unit.
3. Parameters were set for the various antennas as follows:
    - 100 Mhz
        -Time interval: 0.25 seconds
        -Antenna separation: 0.5 metres
        -Sampling frequency: 1581.25 Mhz
        -Time window: 198.6 n/s (10.18m, 344 samples)
    - 250 Mhz
        -Point interval: 0.5 m
        -Antenna separation: 0.36 metres
        -Sampling frequency: 3614.29 Mhz

-Time window: 140.5 n/s (7.18, 536 samples)
- 500 Mhz
  -Point interval: 0.04m
  -Antenna separation: 0.18 metres
  -Sampling frequency: 7535.71 Mhz
  -Time window: 78.8n/s (14.03m, 624 samples)
- 800 Mhz
  -Point interval: 0.014
  -Antenna separation: 0.14 metres
  -Sampling frequency: 12173.08
  -Time window: 39.6 n/s (2.05m, 512 samples)

4. The transects were walked a minimum of two times (up and back).
5. Data were downloaded and backed up.

Drill-core Sampling
1. Drill-cores were chosen to be sampled at 20 metre intervals along each of the transects (or as close as access would allow).
2. Samples were collected at various depths.
3. Samples were placed into labelled bags, for future lab work.
4. Sample bags were weighed, recording the soils "wet weight".

Soil Moisture
1. Soils were placed into an oven at 105°C for 7 days (until no further weight change).
2. Samples were weighed.
3. Dry weight was recorded.
4. Dry weight was compared to wet weight with the difference being divided by the initial wet weight to give a moisture percentage for each sample.

EC 1:5
1. 5 grams of soil (<2mm) were weighed and placed into a vial for each of the samples collected during the drilling program.
2. 25 mL of reverse-osmosis (RO) water were added to each of the vials.
3. Vials were sealed up with a lid, before being placed onto a rotating drum.
4. Sampled were then rotated for 1 hour at 25 RPM, so as to release the salts.
5. Samples were the allowed to rest for 30 minutes.
6. A conductivity meter was then used to measure the conductivity of the samples, providing an indication on the salinities of the various soil profiles.

Data Processing

<u>Resistivity</u>

1. Flash Data Check

    -The first step was to open "flashdatacheck.exe" and load the file to be processed.
    -Check the data.
    -once satisfied with the data an input file was generated.
    -This process was repeated for all of the spreads that were used.

2. Files were then merged into batches of three using Merge_inv_INP64_qw.exe to produce continuous data files for inversion.

3. The merged files were then opened in a text editor and the parameters were set as shown in figure below.

4. Merged data sets were inverted using flash2res2dinv.exe to produce an output file in the form of a surfer grid file.

5. The grid files were then opened in surfer to produce inverted conductivity depth sections.

6. To better demonstrate the large variability in resistivity, the data was then converted into log form suing Surfer 8's math function.

<u>DualEM-421</u>

The Dual EM and EM34 data was processed by John Triantafilis using EM4 soil, which is a software package developed by EMTOMO. This program allows the inversion of σ_a acquired at low induction numbers (LIN) to be possible, and works by inverting the conductivities to produce conductivity depth sections (Triantafilis et al. 2013). The inverted data was then converted to log scale in Microsoft Excel. This was then converted to a csv file, allowing Golden Software's Surfer 8 to grid the data using Kriging gridding method. The data was then contoured using Surfer 8.

<u>GPR</u>

1. Data was imported into Reflex W
2. Subtract mean (deWow)
3. Static correction was picked at the first positive phase amplitude received
4. Background removal was applied to remove background signal
5. F-K Stolt migration (using V=0.14 m/ns) was applied
6. Data was enveloped, to correct all values to positive phase amplitude
7. Running average was applied to smooth data (20 samples for 500 MHz)
8. Trace headers were aligned using GPS co-ordinates

<u>Soil Data</u>
1. The soil data collected were entered into Microsoft excel.
2. Microsoft Excel files were converted to csv files
3. Encom PA (Profile Analyst) was used to produce drill-hole data for moisture (weight %) and EC 1:5 (µS/cm)

APPENDIX B: TRANSECT 1 (ROCKY PADDOCK) SOIL DATA

Drillhole	Distance (m)	easting	northing	Elevation	Depthfrom (m)	Depthto (m)	Moisture (wt%)	EC 1:5 (μS/cm)	% >2mm	%<2mm	strength	rego
DH1	0	311270	6156095	442.4	0	-0.3	7.14152038	81.00	0.20734	0.792663	VW	
	0	311270	6156095	442.4	-0.3	-0.6	10.97190956	58.10	0.25783	0.74217	W	
	0	311270	6156095	442.4	-0.6	-0.9	3.379098118	39.10	0.14115	0.858852	L	
	0	311270	6156095	442.4	-0.9	-1.2	-0.417623721	30.20	0.01971	0.980291	L	
	0	311270	6156095	442.4	-1.2	-1.5	-0.925976659	34.70	0.00908	0.990925	L	

Drillhole	Distance	easting	northing	Elevation	Depthfrom (m)	Depthto (m)	Moisture (wt%)	EC 1:5 (μS/cm)	% >2mm	%<2mm	strength	rego
DH2	20	311258	6156079	441.7	0	-0.3	1.948869309	113.70	0.3244	0.675602	VW	
	20	311258	6156079	441.7	-0.3	-0.6	8.928170415	65.70	0.49348	0.506521	W	
	20	311258	6156079	441.7	-0.6	-0.9	2.333793951	43.20	0.414	0.585997	VF	
	20	311258	6156079	441.7	-0.9	-1.2	8.541598695	61.30	0.57237	0.42763	S	
	20	311258	6156079	441.7	-1.2	-1.5	3.964439631	76.60	0.44928	0.550721	S	

Drillhole	Distance	easting	northing	Elevation	Depthfrom (m)	Depthto (m)	Moisture (wt%)	EC 1:5 (μS/cm)	% >2mm	%<2mm	strength	rego
DH3	40	311244	6156064	441.6	0	-0.3	3.509087637	83.00	0.1699	0.830095	VL	
	40	311244	6156064	441.6	-0.3	-0.6	7.939854207	50.40	0.38048	0.619518	W	
	40	311244	6156064	441.6	-0.6	-0.9	6.673146164	37.20	0.40024	0.599762	F	
	40	311244	6156064	441.6	-0.9	-1.2	10.8977222	50.00	0.49431	0.505688	F	
	40	311244	6156064	441.6	-1.2	-1.5	7.447008654	51.50	0.36678	0.633219	W	
	40	311244	6156064	441.6	-1.5	-1.9	6.434669672	43.00	0.30533	0.694672	W	

Drillhole	Distance	easting	northing	Elevation	Depthfrom (m)	Depthto (m)	Moisture (wt%)	EC 1:5 (µS/cm)	% >2mm	%<2mm	strength	rego
DH4	60	311230	6156051	441.7	0	-0.3	-0.168062091	81.30	0.35398	0.646023	L	A=0-30
	60	311230	6156051	441.7	-0.3	-0.6	7.348960727	47.20	0.37603	0.623967	VF	B=30-60
	60	311230	6156051	441.7	-0.6	-0.9	3.492737872	31.80	0.3234	0.6766	F	C=60-125
	60	311230	6156051	441.7	-0.9	-1.2	3.240235959	29.00	0.30704	0.692959	F	
	60	311230	6156051	441.7	-1.2	-1.35	2.712540514	38.70	0.2537	0.7463	W	

Drillhole	Distance	easting	northing	Elevation	Depthfrom (m)	Depthto (m)	Moisture (wt%)	EC 1:5 (µS/cm)	% >2mm	%<2mm	strength	rego
DH5	80	311215	6156038	440.4	0	-0.3	3.856485741	199.80	0.27411	0.725888	L	A=0-30
	80	311215	6156038	440.4	-0.3	-0.6	13.0116066	53.10	0.58604	0.41396	VF	B=30-60
	80	311215	6156038	440.4	-0.6	-0.9	9.825600695	39.00	0.58364	0.416363	VF	C=60-150
	80	311215	6156038	440.4	-0.9	-1.2	2.88473262	26.60	0.27148	0.728517	W	
	80	311215	6156038	440.4	-1.2	-1.5	3.178958041	33.50	1	0	W	

Drillhole	Distance	easting	northing	Elevation	Depthfrom (m)	Depthto (m)	Moisture (wt%)	EC 1:5 (µS/cm)	% >2mm	%<2mm	strength	rego
DH6	100	311201	6156024	439.5	0	-0.3	1.511538192	100.60	0.16551	0.834488	L	A=0-50
	100	311201	6156024	439.5	-0.3	-0.6	11.98791932	58.00	0.34726	0.652744	F	B=50-60
	100	311201	6156024	439.5	-0.6	-0.9	14.00841974	48.10	0.32962	0.67038	VF	C=90-180
	100	311201	6156024	439.5	-0.9	-1.2	10.04273021	40.40	0.3003	0.699697	F	
	100	311201	6156024	439.5	-1.2	-1.5	5.544308457	33.50	0.21311	0.786893	W	
	100	311201	6156024	439.5	-1.5	-1.8	4.77058319	28.70	0.37056	0.629436	W	

Drillhole	Distance	easting	northing	Elevation	Depthfrom (m)	Depthto (m)	Moisture (wt%)	EC 1:5 (μS/cm)	% >2mm	%<2mm	strength	rego
DH7	120	311185	6156011	439.7	0	-0.3	2.860976019	107.40	0.18214	0.817861	L	A=0-30
	120	311185	6156011	439.7	-0.3	-0.6	7.775384711	55.90	0.32285	0.677155	VF	B=30-100
	120	311185	6156011	439.7	-0.6	-0.9	12.97316384	48.50	0.45472	0.545283	F	C=100-200
	120	311185	6156011	439.7	-0.9	-1.2	7.582887701	34.20	0.1231	0.876898	F	
	120	311185	6156011	439.7	-1.2	-1.5	5.976802365	35.60	0.21535	0.784646	W	
	120	311185	6156011	439.7	-1.5	-2	7.602822697	34.20	0.24423	0.755775	W	

Drillhole	Distance	easting	northing	Elevation	Depthfrom (m)	Depthto (m)	Moisture (wt%)	EC 1:5 (μS/cm)	% >2mm	%<2mm	strength	rego
DH8	140	311170	6155999	440.5	0	-0.3	1.477678726	70.20	0.03571	0.964286	L	A1=0-30
	140	311170	6155999	440.5	-0.3	-0.6	4.4066927	45.30	0.25569	0.744313	L/F	A2=30-50
	140	311170	6155999	440.5	-0.6	-0.9	15.75805714	58.40	0.51549	0.484507	VF	B=50-120
	140	311170	6155999	440.5	-0.9	-1.2	N/A	58.20	0.4956	0.504399	F	C=120-200
	140	311170	6155999	440.5	-1.2	-1.5	11.98633027	55.10	0.36888	0.631124	F	
	140	311170	6155999	440.5	-1.5	-2	7.265956792	41.80	0.28811	0.711893	W	

Drillhole	Distance	easting	northing	Elevation	Depthfrom (m)	Depthto (m)	Moisture (wt%)	EC 1:5 (µS/cm)	% >2mm	%<2mm	strength	rego
DH9	160	311155	6155987	441.3	0	-0.3	1.834168479	135.60	0.21126	0.788739	L	
	160	311155	6155987	441.3	-0.3	-0.6	13.16326531	60.50	0.35907	0.64093	VF	
	160	311155	6155987	441.3	-0.6	-0.9	12.3509683	57.10	0.42442	0.57558	VF	
	160	311155	6155987	441.3	-0.9	-1.2	12.48978882	60.40	0.27956	0.720441	F	
	160	311155	6155987	441.3	-1.2	-1.5	2.964597811	38.60	0.23814	0.76186	F	
	160	311155	6155987	441.3	-1.5	-2	7.665340359	31.20	0.34647	0.653532	W	
	160	311155	6155987	441.3	-2	-2.5	11.55697854	34.80	0.36987	0.63013	W	
	160	311155	6155987	441.3	-2.5	-3	18.14667268	76.20	0.29416	0.705842	W	
	160	311155	6155987	441.3	-3	-3.5	16.34165755	90.60	0.28815	0.711855	W	
	160	311155	6155987	441.3	-3.5	-4	16.46103345	123.90	0.13322	0.866776	W	
	160	311155	6155987	441.3	-4	-4.5	11.24092396	100.00	0.21943	0.780571	W	
	160	311155	6155987	441.3	-4.5	-4.7	9.208257378	117.00	0.24181	0.758188	W	

Drillhole	Distance	easting	northing	Elevation	Depthfrom (m)	Depthto (m)	Moisture (wt%)	EC 1:5 (µS/cm)	% >2mm	%<2mm	strength	rego
DH10	180	311139	6155973	443.7	0	-0.3	3.117138365	138.40	0.05558	0.944421	L	A1=0-15
	180	311139	6155973	443.7	-0.3	-0.6	4.280940955	51.90	0.73949	0.260508	VF	A2=15-40
	180	311139	6155973	443.7	-0.6	-0.9	9.719410634	62.20	0.73484	0.26516	S/VF	B=40-70
	180	311139	6155973	443.7	-0.9	-1.2	11.90130881	62.30	0.50937	0.490631	R	C=70-90
												R=90-120

Drillhole	Distance	easting	northing	Elevation	Depthfrom (m)	Depthto (m)	Moisture (wt%)	EC 1:5 (µS/cm)	% >2mm	%<2mm	strength	rego
DH11	200	311124	6155961	446.3	0	-0.3	1.314249028	108.90	0.09223	0.907765	L	A1=0-10
	200	311124	6155961	446.3	-0.3	-0.6	13.29367645	63.10	0.33417	0.66583	VF/L	A2=10-30
	200	311124	6155961	446.3	-0.6	-0.9	15.23499974	68.30	0.56429	0.435708	VF/L	B2=30-140
	200	311124	6155961	446.3	-0.9	-1.2	11.33839432	61.30	0.65757	0.342428	VF/L	C=140-330
	200	311124	6155961	446.3	-1.2	-1.5	10.97876436	58.40	0.55448	0.445517	F	
	200	311124	6155961	446.3	-1.5	-2	10.60815822	60.40	0.51247	0.487532	F	
	200	311124	6155961	446.3	-2	-2.5	10.90538041	55.40	0.43962	0.560384	VW	
	200	311124	6155961	446.3	-2.5	-3	11.45547669	44.90	0.41541	0.584594	W	
	200	311124	6155961	446.3	-3	-3.3	6.672453076	76.00	0.40905	0.590952	L	

Drillhole	Distance	easting	northing	Elevation	Depthfrom (m)	Depthto (m)	Moisture (wt%)	EC 1:5 (µS/cm)	% >2mm	%<2mm	strength	rego
DH12	220	311108	6155948	449	0	-0.3	2.308315335	183.20	0.26968	0.730321	L	A1=0-10
	220	311108	6155948	449	-0.3	-0.6	10.04602296	104.80	0.31211	0.687891	F	A2=10-30
	220	311108	6155948	449	-0.6	-0.9	12.378922	76.90	0.60272	0.397282	VF	B2=30-90
	220	311108	6155948	449	-0.9	-1.2	11.34196185	75.40	0.5202	0.479799	R	R=90-120
	220	311108	6155948	449	-1.2	-1.5	8.941696996	92.40	0.43303	0.566973	S	

Drillhole	Distance	easting	northing	Elevation	Depthfrom (m)	Depthto (m)	Moisture (wt%)	EC 1:5 (µS/cm)	% >2mm	%<2mm	strength	rego
DH13	240	311093	6155937	451.7	0	-0.3	2.200155159	104.80	0.45935	0.540654	L/W	A1=0-10
	240	311093	6155937	451.7	-0.3	-0.6	13.63825874	104.00	0.32318	0.676817	VF	A2=10-20
	240	311093	6155937	451.7	-0.6	-0.9	8.542287777	59.30	0.23595	0.764049	F	B2=20-80
	240	311093	6155937	451.7	-0.9	-1.2	5.628509328	99.30	0.17202	0.827981	F	C=80-170
	240	311093	6155937	451.7	-1.2	-1.5	7.401138188	151.10	0.21002	0.789981	F	
	240	311093	6155937	451.7	-1.5	-1.7	3.854051493	97.00	0.19415	0.805853	F	

Drillhole	Distance	easting	northing	Elevation	Depthfrom (m)	Depthto (m)	Moisture (wt%)	EC 1:5 (µS/cm)	% >2mm	%<2mm	strength	rego
DH14	260	311078	6155925	N/A	0	-0.3	8.072297581	119.50	0.3827	0.617303	L	A1=0-5
	260	311078	6155925	N/A	-0.3	-0.6	12.75336091	89.30	0.28696	0.713036	VF	A2=5-10
	260	311078	6155925	N/A	-0.6	-0.9	7.661279761	54.60	0.13435	0.86565	VF	B2=10-80
	260	311078	6155925	N/A	-0.9	-1.2	4.886125566	47.20	0.037	0.962999	VF	C=80-280
	260	311078	6155925	N/A	-1.2	-1.5	4.119951895	51.50	0.01247	0.987526	F	R=280-300
	260	311078	6155925	N/A	-1.5	-2	5.179396248	75.10	0.13005	0.869953	F	
	260	311078	6155925	N/A	-2	-2.5	6.153777798	228.00	0.23901	0.76099	W	
	260	311078	6155925	N/A	-2.5	-3	6.602927158	188.20	0.15865	0.841348	VF	

APPENDIX C: TRANSECT 2 (CHALKIES) SOIL DATA

Drillhole	Distance	easting	northing	Elevation	Depthfrom (m)	Depthto (m)	Moisture (wt%)	EC 1:5 (μS/cm)	% >2mm	%<2mm	strength	rego
DH1	0	312622	6153444	451.24	0	-0.3	11.82760502	121.50	0.49403	0.50597	L	A1=0-7
	0	312622	6153444	451.24	-0.3	-0.6	13.64103736	78.30	0.24225	0.75775	S	A2=7-20
	0	312622	6153444	451.24	-0.6	-0.9	11.78977273	140.10	0.00233	0.99767	VF	B2=20-70
	0	312622	6153444	451.24	-0.9	-1.2	11.45975443	231.00	0.00651	0.99349	R	C=70-80
	0	312622	6153444	451.24	-1.2	-1.5	14.19468547	287.00	0.02151	0.97849	R	R=80-180
	0	312622	6153444	451.24	-1.5	-1.9	14.54948798	346.00	0.15693	0.84307	R	

Drillhole	Distance	easting	northing	Elevation	Depthfrom (m)	Depthto (m)	Moisture (wt%)	EC 1:5 (μS/cm)	% >2mm	%<2mm	strength	rego
DH2	20	312641	6153440	449.64	0	-0.3	7.064999331	150.00	0.35158	0.64842	L	A1=0-8
	20	312641	6153440	449.64	-0.3	-0.6	12.49073388	69.30	0.21558	0.78442	VF	A2=8-20
	20	312641	6153440	449.64	-0.6	-0.9	9.120193276	69.90	0.0101	0.9899	VF	B2=20-60
	20	312641	6153440	449.64	-0.9	-1.2	8.628439864	102.90	0.01797	0.98203	VF	C=60-70
	20	312641	6153440	449.64	-1.2	-1.5	6.88892096	171.90	0.05693	0.94307	R/L	R=70-170
	20	312641	6153440	449.64	-1.5	-1.7	4.510530098	143.80	0.07892	0.92108	R/L	

Drillhole	Distance	easting	northing	Elevation	Depthfrom (m)	Depthto (m)	Moisture (wt%)	EC 1:5 (µS/cm)	% >2mm	%<2mm	strength	rego
DH3	33	312653	6153446	447.45	0	-0.3	4.126740192	92.60	0.49927	0.50073	L	A1=0-10
	33	312653	6153446	447.45	-0.3	-0.6	11.41483169	65.10	0.01541	0.98459	F	A2=10-30
	33	312653	6153446	447.45	-0.6	-0.9	7.513061031	55.10	0.05144	0.94856	F	B2=30-90
	33	312653	6153446	447.45	-0.9	-1.2	3.267272147	41.40	0.25743	0.74257	F	C=90-150
	33	312653	6153446	447.45	-1.2	-1.5	2.938427149	46.70	0.36162	0.63838	R	R=150-480
	33	312653	6153446	447.45	-1.5	-2	2.654815508	108.00	0.17056	0.82944	W	
	33	312653	6153446	447.45	-2	-2.5	5.132156289	176.50	0.39522	0.60478	W/F	
	33	312653	6153446	447.45	-2.5	-3	8.140798146	156.20	0.22186	0.77814	W/F	
	33	312653	6153446	447.45	-3	-3.5	10.52724201	84.10	0.173	0.827	L	
	33	312653	6153446	447.45	-3.5	-4	11.07227898	94.10	0.09759	0.90241	W	
	33	312653	6153446	447.45	-4	-4.5	8.387563268	79.70	0.19144	0.80856	F	
	33	312653	6153446	447.45	-4.5	-4.8	7.570018365	68.50	0.3728	0.6272	VF	

Drillhole	Distance	easting	northing	Elevation	Depthfrom (m)	Depthto (m)	Moisture (wt%)	EC 1:5 (µS/cm)	% >2mm	%<2mm	strength	rego
DH4	40	312660	6153442	446.44	0	-0.3	5.065581185	67.80	0.36613	0.63387	L/F	A1=0-10
	40	312660	6153442	446.44	-0.3	-0.6	11.01568335	48.10	0.17241	0.82759	VF	A2=10-20
	40	312660	6153442	446.44	-0.6	-0.9	7.00592319	40.80	0.15485	0.84515	F	B2=20-80
	40	312660	6153442	446.44	-0.9	-1.2	5.222335247	43.80	0.00898	0.99102	VF	C=80-120
	40	312660	6153442	446.44	-1.2	-1.45	5.555152658	66.10	0.41943	0.58057	R/L	R=120-145

Drillhole	Distance	easting	northing	Elevation	Depthfrom (m)	Depthto (m)	Moisture (wt%)	EC 1:5 (µS/cm)	% >2mm	%<2mm	strength	rego
DH5	60	312680	6153437	443.39	0	-0.3	2.936362118	93.00	0.55966	0.44034	L/R	A=0-30
	60	312680	6153437	443.39	-0.3	-0.6	9.990212528	121.00	0.53452	0.46548	F	B2=30-80
	60	312680	6153437	443.39	-0.6	-0.9	7.354564245	65.10	0.6135	0.3865	VF	C=80-220
	60	312680	6153437	443.39	-0.9	-1.2	4.989148663	34.40	0.67317	0.32683	VF	R=220-240
	60	312680	6153437	443.39	-1.2	-1.5	5.183312263	42.10	0.45402	0.54598	R/L	
	60	312680	6153437	443.39	-1.5	-2	3.856722034	38.00	0.55064	0.44936	VS/L	
	60	312680	6153437	443.39	-2	-2.4	2.519417076	26.30	0.44583	0.55417	VS/L	

Drillhole	Distance	easting	northing	Elevation	Depthfrom (m)	Depthto (m)	Moisture (wt%)	EC 1:5 (µS/cm)	% >2mm	%<2mm	strength	rego
DH6	80	312699	6153439	441.27	0	-0.3	5.565767974	57.30	0.03179	0.96821	L	A1=0-10
	80	312699	6153439	441.27	-0.3	-0.6	7.50851454	38.30	0.29914	0.70086	F	A2=10-50
	80	312699	6153439	441.27	-0.6	-0.9	11.44971064	36.00	0.0401	0.9599	VF	B2=50-85
	80	312699	6153439	441.27	-0.9	-1.2	2.803459588	25.40	0.30543	0.69457	VF	C=85-730
	80	312699	6153439	441.27	-1.2	-1.5	2.672463397	33.80	0.28207	0.71793	F/L	
	80	312699	6153439	441.27	-1.5	-2	6.322902894	79.00	0.57792	0.42208	F	
	80	312699	6153439	441.27	-2	-2.5	7.097999894	44.60	0.03018	0.96982	F/L	
	80	312699	6153439	441.27	-2.5	-3	8.087485362	48.20	0.01906	0.98094	VW	
	80	312699	6153439	441.27	-3	-3.5	7.206498127	45.70	0.03201	0.96799	VW	
	80	312699	6153439	441.27	-3.5	-4	5.958838762	43.00	0.06408	0.93592	W	
	80	312699	6153439	441.27	-4	-4.5	6.680689103	47.90	0.00037	0.99963	L	
	80	312699	6153439	441.27	-4.5	-5	9.643965916	67.00	0	1	VW	
	80	312699	6153439	441.27	-5	-5.5	9.705407587	75.80	0	1	W	
	80	312699	6153439	441.27	-5.5	-6	11.98194501	86.30	0.0191	0.9809	W	
	80	312699	6153439	441.27	-6	-6.5	11.06873112	85.80	0	1	W	
	80	312699	6153439	441.27	-6.5	-7	10.68777576	80.80	0	1	W	
	80	312699	6153439	441.27	-7	-7.3	8.47442417	69.80	0	1	W	

Drillhole	Distance	easting	northing	Elevation	Depthfrom (m)	Depthto (m)	Moisture (wt%)	EC 1:5 (µS/cm)	% >2mm	%<2mm	strength	rego
DH7	100	312721	6153433	439.66	0	-0.3	6.263993752	70.00	0.47064	0.52936	L/F	A1=0-5
	100	312721	6153433	439.66	-0.3	-0.6	13.92941853	65.40	0.04021	0.95979	S	A2=5-20
	100	312721	6153433	439.66	-0.6	-0.9	8.722812015	34.60	0.02198	0.97802	VF	B2=20-65
	100	312721	6153433	439.66	-0.9	-1.2	5.780063156	28.10	0.27383	0.72617	S	C=65-590
	100	312721	6153433	439.66	-1.2	-1.5	2.976862996	30.00	0	1	VF	
	100	312721	6153433	439.66	-1.5	-2	3.130182731	26.20	0.05326	0.94674	VF	
	100	312721	6153433	439.66	-2	-2.5	2.949695122	29.10	0.16907	0.83093	VF	
	100	312721	6153433	439.66	-2.5	-3	5.774178696	31.40	0.23172	0.76828	F	
	100	312721	6153433	439.66	-3	-3.5	6.483790524	27.40	0.05452	0.94548	F	
	100	312721	6153433	439.66	-3.5	-4	6.828505473	24.10	0	1	W	
	100	312721	6153433	439.66	-4	-4.5	6.558156113	26.10	0.00742	0.99258	W	
	100	312721	6153433	439.66	-4.5	-5	6.439415003	27.60	0.01033	0.98967	W	
	100	312721	6153433	439.66	-5	-5.5	7.13972242	30.00	0.00907	0.99093	W	
	100	312721	6153433	439.66	-5.5	-5.9	8.464691047	27.00	0.03731	0.96269	F	

Drillhole	Distance	easting	northing	Elevation	Depthfrom (m)	Depthto (m)	Moisture (wt%)	EC 1:5 (µS/cm)	% >2mm	%<2mm	strength	rego
DH8	120	312740	6153435	441.27	0	-0.3	1.169275422	34.60	0.51153	0.48847	S	A1=0-5
	120	312740	6153435	441.27	-0.3	-0.6	2.837975701	31.20	0.17775	0.82225	S/R	A2=5-10
	120	312740	6153435	441.27	-0.6	-0.8	3.529883674	31.40	0.04964	0.95036	S/R	C/R=10-80

Drillhole	Distance	easting	northing	Elevation	Depthfrom (m)	Depthto (m)	Moisture (wt%)	EC 1:5 (µS/cm)	% >2mm	%<2mm	strength	rego
DH9	140	312759	6153439	441.36	0	-0.3	3.241061478	36.90	0.35391	0.64609	F	A1=0-7
	140	312759	6153439	441.36	-0.3	-0.6	5.057506517	36.50	0.0879	0.9121	F	A2=7-30
	140	312759	6153439	441.36	-0.6	-0.95	9.486865685	43.30	0.15542	0.84458	VF	B=30-50
												C=50-95

Drillhole	Distance	easting	northing	Elevation	Depthfrom (m)	Depthto (m)	Moisture (wt%)	EC 1:5 (µS/cm)	% >2mm	%<2mm	strength	rego
DH10	160	312779	6153436	442.14	0	-0.3	5.437606946	46.60	0.22687	0.77313	L	A1=0-7
	160	312779	6153436	442.14	-0.3	-0.6	13.31014396	45.30	0.25291	0.74709	W	A2=7-22
	160	312779	6153436	442.14	-0.6	-0.9	10.82184447	30.90	0.20251	0.79749	F	B=22-130
	160	312779	6153436	442.14	-0.9	-1.2	11.32667317	32.30	0.06863	0.93137	F	C=130-500
	160	312779	6153436	442.14	-1.2	-1.5	10.78499884	36.20	0.00178	0.99822	F	R=500-520
	160	312779	6153436	442.14	-1.5	-2	7.018864481	32.20	0.35659	0.64341	F	
	160	312779	6153436	442.14	-2	-2.5	10.94073053	31.10	0.00592	0.99408	W	
	160	312779	6153436	442.14	-2.5	-3	13.16750528	44.30	0	1	W	
	160	312779	6153436	442.14	-3	-3.5	12.79931158	34.10	0.00488	0.99512	W	
	160	312779	6153436	442.14	-3.5	-4	11.754716	29.90	0	1	W	
	160	312779	6153436	442.14	-4	-4.5	13.63927087	30.90	0.03012	0.96988	VW	
	160	312779	6153436	442.14	-4.5	-5	12.87962452	33.00	0.18052	0.81948	R	
	160	312779	6153436	442.14	-5	-5.2	11.90466556	40.80	0.04327	0.95673	R	

Drillhole	Distance	easting	northing	Elevation	Depthfrom (m)	Depthto (m)	Moisture (wt%)	EC 1:5 (µS/cm)	% >2mm	%<2mm	strength	rego
DH11	180	312798	6153437	437.04	0	-0.3	4.17104802	47.30	0.48205	0.51795	W	A1=0-7
	180	312798	6153437	437.04	-0.3	-0.6	8.185700728	33.50	0.05968	0.94032	VF	A2=7-10
	180	312798	6153437	437.04	-0.6	-0.8	7.292066575	30.10	0.36373	0.63627	R	B=10-50

Drillhole	Distance	easting	northing	Elevation	Depthfrom (m)	Depthto (m)	Moisture (wt%)	EC 1:5 (µS/cm)	% >2mm	%<2mm	strength	rego
DH12	200	312817	6153439	432.71	0	-0.3	3.575053569	72.80	0.43129	0.56871	L	A1=0-30
	200	312817	6153439	432.71	-0.3	-0.6	12.34294842	46.30	0.40532	0.59468	VF	B1=30-50
	200	312817	6153439	432.71	-0.6	-0.9	11.7807154	39.00	0.21801	0.78199	VF	B2=50-100
	200	312817	6153439	432.71	-0.9	-1.2	10.8839034	45.60	0.39365	0.60635	F	C=100-120
	200	312817	6153439	432.71	-1.2	-1.4	10.23454158	56.10	0.43586	0.56414	R	R=120-140

Drillhole	Distance	easting	northing	Elevation	Depthfrom (m)	Depthto (m)	Moisture (wt%)	EC 1:5 (µS/cm)	% >2mm	%<2mm	strength	rego
DH13	220	312834	6153432	433.18	0	-0.3	3.711515457	59.40	0.48142	0.51858	L	A1=0-15
	220	312834	6153432	433.18	-0.3	-0.6	11.35771408	42.90	0.27558	0.72442	W	A2=15-35
	220	312834	6153432	433.18	-0.6	-0.9	12.40386419	34.60	0.39309	0.60691	W	B2=35-135
	220	312834	6153432	433.18	-0.9	-1.2	8.778478569	30.40	0.10541	0.89459	S	C=135-210
	220	312834	6153432	433.18	-1.2	-1.5	8.568046619	35.40	0.08032	0.91968	S	R=210-225
	220	312834	6153432	433.18	-1.5	-2	12.23256279	64.20	0.29876	0.70124	S	
	220	312834	6153432	433.18	-2	-2.25	10.9382099	53.20	0.45979	0.54021	R	

Drillhole	Distance	easting	northing	Elevation	Depthfrom (m)	Depthto (m)	Moisture (wt%)	EC 1:5 (μS/cm)	% >2mm	%<2mm	strength	rego
DH14	240	312859	6153431	430.16	0	-0.3	2.495603787	46.30	0.27746	0.72254	W	A1=0-5
	240	312859	6153431	430.16	-0.3	-0.6	7.423269094	32.10	0.14773	0.85227	F	A2=5-35
	240	312859	6153431	430.16	-0.6	-0.9	10.85890239	32.60	0.00955	0.99045	VF	B2=35-110
	240	312859	6153431	430.16	-0.9	-1.2	4.919571046	34.20	0.08673	0.91327	F	C=110-230
	240	312859	6153431	430.16	-1.2	-1.5	3.603931562	31.90	0.00461	0.99539	VF	
	240	312859	6153431	430.16	-1.5	-2	4.352209393	47.60	0.01331	0.98669	S	
	240	312859	6153431	430.16	-2	-2.3	6.500515641	39.50	0.02528	0.97472	VS	

Drillhole	Distance	easting	northing	Elevation	Depthfrom (m)	Depthto (m)	Moisture (wt%)	EC 1:5 (μS/cm)	% >2mm	%<2mm	strength	rego
DH15	260	312879	6153430	427.72	0	-0.3	4.92894456	57.90	0.38445	0.61555	n/a	A1=0-10
	260	312879	6153430	427.72	-0.3	-0.6	9.892921098	38.30	0.24021	0.75979	n/a	A2=10-20
	260	312879	6153430	427.72	-0.6	-0.9	10.62750898	47.20	0.19614	0.80386	n/a	B2=20-75
	260	312879	6153430	427.72	-0.9	-1.2	7.684657207	47.60	0.17787	0.82213	n/a	C=75-135
	260	312879	6153430	427.72	-1.2	-1.35	7.844983133	73.40	0.46727	0.53273	n/a	

Drillhole	Distance	easting	northing	Elevation	Depthfrom (m)	Depthto (m)	Moisture (wt%)	EC 1:5 (μS/cm)	% >2mm	%<2mm	strength	rego
DH16	280	312898	6153426	427.57	0	-0.3	2.270916335	54.20	0.19795	0.80205	n/a	A1=0-10
	280	312898	6153426	427.57	-0.3	-0.6	9.349445284	40.60	0.01016	0.98984	n/a	A2=10-20
	280	312898	6153426	427.57	-0.6	-0.9	8.647248603	36.10	0.13282	0.86718	n/a	B1=20-35
	280	312898	6153426	427.57	-0.9	-1.2	8.276869935	36.30	0.00602	0.99398	n/a	B2=35-100
	280	312898	6153426	427.57	-1.2	-1.5	5.952258639	42.50	0.00674	0.99326	n/a	C=100-715
	280	312898	6153426	427.57	-1.5	-2	5.599707682	49.90	0.02803	0.97197	n/a	
	280	312898	6153426	427.57	-2	-2.5	10.62773864	63.90	0.01356	0.98644	n/a	
	280	312898	6153426	427.57	-2.5	-3	13.74822785	88.60	0.01172	0.98828	n/a	
	280	312898	6153426	427.57	-3	-3.5	14.12760417	88.70	0.00174	0.99826	n/a	
	280	312898	6153426	427.57	-3.5	-4	13.56940335	115.70	0	1	n/a	
	280	312898	6153426	427.57	-4	-4.5	17.44232398	114.30	0	1	n/a	
	280	312898	6153426	427.57	-4.5	-5	17.25873677	108.60	0.00238	0.99762	n/a	
	280	312898	6153426	427.57	-5	-5.5	16.14836594	94.70	0.01348	0.98652	n/a	
	280	312898	6153426	427.57	-5.5	-6	18.28558538	115.70	0.02277	0.97723	n/a	
	280	312898	6153426	427.57	-6	-6.5	17.54675138	124.40	0.01674	0.98326	n/a	
	280	312898	6153426	427.57	-6.5	-7	19.27550681	121.10	0.00421	0.99579	n/a	
	280	312898	6153426	427.57	-7	-7.15	19.24509383	125.50	0	1	n/a	

Drillhole	Distance	easting	northing	Elevation	Depthfrom (m)	Depthto (m)	Moisture (wt%)	EC 1:5 (µS/cm)	% >2mm	%<2mm	strength	rego
DH17	300	312917	6153429	424.34	0	-0.3	10.18875193	66.70	0.46667	0.53333	n/a	A1=0-10
	300	312917	6153429	424.34	-0.3	-0.6	9.351329018	42.60	0.44322	0.55678	n/a	B2=10-80
	300	312917	6153429	424.34	-0.6	-0.85	9.514943655	58.50	0.12216	0.87784	n/a	C=80-85

Drillhole	Distance	easting	northing	Elevation	Depthfrom (m)	Depthto (m)	Moisture (wt%)	EC 1:5 (µS/cm)	% >2mm	%<2mm	strength	rego
DH18	320	312938	6153428	423.47	0	-0.3	10.15234364	97.10	0.5719	0.4281	n/a	A1=0-12
	320	312938	6153428	423.47	-0.3	-0.6	15.14724269	62.20	0.30041	0.69959	n/a	A2=12-20
	320	312938	6153428	423.47	-0.6	-0.9	10.57556305	61.40	0	1	n/a	B2=20-90
	320	312938	6153428	423.47	-0.9	-1.05	9.680923286	72.00	0.44453	0.55547	n/a	C=90-105

Drillhole	Distance	easting	northing	Elevation	Depthfrom (m)	Depthto (m)	Moisture (wt%)	EC 1:5 (µS/cm)	% >2mm	%<2mm	strength	rego
DH19	340	312958	6153427	421.23	0	-0.3	8.19883796	61.40	0.47088	0.52912	n/a	A1=0-5
	340	312958	6153427	421.23	-0.3	-0.6	14.85311507	44.50	0.0043	0.9957	n/a	A2=5-15
	340	312958	6153427	421.23	-0.6	-0.9	12.22585457	40.10	0.01594	0.98406	n/a	B2=15-120
	340	312958	6153427	421.23	-0.9	-1.2	12.95593678	41.40	0	1	n/a	C=120-330
	340	312958	6153427	421.23	-1.2	-1.5	13.80823677	52.50	0.04657	0.95343	n/a	
	340	312958	6153427	421.23	-1.5	-2	17.20964717	65.80	0.15055	0.84945	n/a	
	340	312958	6153427	421.23	-2	-2.5	18.42056191	82.20	0.02462	0.97538	n/a	
	340	312958	6153427	421.23	-2.5	-3	12.7186214	89.60	0.35176	0.64824	n/a	
	340	312958	6153427	421.23	-3	-3.3	13.22089047	128.50	0.4936	0.5064	n/a	

Drillhole	Distance	easting	northing	Elevation	Depthfrom (m)	Depthto (m)	Moisture (wt%)	EC 1:5 (μS/cm)	% >2mm	%<2mm	strength	rego
DH20	360	312978	6153426	418.81	0	-0.3	4.580712384	45.20	0.10124	0.89876	L	A1=0-25
	360	312978	6153426	418.81	-0.3	-0.6	7.708141725	50.60	0.36453	0.63547	W	A2=25-30
	360	312978	6153426	418.81	-0.6	-0.9	13.53479304	43.40	0.06653	0.93347	F	B1=30-50
	360	312978	6153426	418.81	-0.9	-1.2	8.840009165	41.20	0.06792	0.93208	VF	B2=50-80
	360	312978	6153426	418.81	-1.2	-1.5	9.875064179	52.40	0.24513	0.75487	F	C=80-140
												R=140-150

Drillhole	Distance	easting	northing	Elevation	Depthfrom (m)	Depthto (m)	Moisture (wt%)	EC 1:5 (μS/cm)	% >2mm	%<2mm	strength	rego
DH21	400	313019	6153422	420.58	0	-0.3	5.085910653	52.80	0.67612	0.32388	L	A1=0-15
	400	313019	6153422	420.58	-0.3	-0.6	16.41250652	60.20	0.43461	0.56539	F	A2=15-25
	400	313019	6153422	420.58	-0.6	-0.9	17.2761627	63.10	0.29198	0.70802	F	B2=25-140
	400	313019	6153422	420.58	-0.9	-1.2	16.80401044	76.60	0.317	0.683	VF	R=140-150
	400	313019	6153422	420.58	-1.2	-1.5	15.82024502	129.50	0.65694	0.34306	S	

Drillhole	Distance	easting	northing	Elevation	Depthfrom (m)	Depthto (m)	Moisture (wt%)	EC 1:5 (µS/cm)	% >2mm	%<2mm	strength	rego
DH22	460	313079	6153420	412.85	0	-0.3	3.538499875	70.80	0.43794	0.56206	W	A1=0-5
	460	313079	6153420	412.85	-0.3	-0.6	7.895454793	61.60	0.30308	0.69692	W	A2=5-25
	460	313079	6153420	412.85	-0.6	-0.9	9.993239352	61.80	0.25181	0.74819	S	B2=25-80
	460	313079	6153420	412.85	-0.9	-1.2	9.734972742	56.70	0.11155	0.88845	R/L	C=80-450
	460	313079	6153420	412.85	-1.2	-1.5	9.594837296	79.80	0.50187	0.49813	F	R=450-600
	460	313079	6153420	412.85	-1.5	-2	13.76043979	251.00	0.657	0.343	F	
	460	313079	6153420	412.85	-2	-2.5	8.492692688	231.70	0.17556	0.82444	W	
	460	313079	6153420	412.85	-2.5	-3	9.420770831	449.00	0.06006	0.93994	W/L	
	460	313079	6153420	412.85	-3	-3.5	9.458996481	490.00	0.22462	0.77538	L	
	460	313079	6153420	412.85	-3.5	-4	10.78642715	539.00	0.11812	0.88188	L	
	460	313079	6153420	412.85	-4	-4.5	8.98298797	430.00	0	1	W	
	460	313079	6153420	412.85	-4.5	-5	12.99783369	610.00	0.12467	0.87533	L	
	460	313079	6153420	412.85	-5	-5.5	13.48110701	610.00	0.15106	0.84894	L	
	460	313079	6153420	412.85	-5.5	-6	9.938546302	416.00	0.01553	0.98447	L	

Drillhole	Distance	easting	northing	Elevation	Depthfrom (m)	Depthto (m)	Moisture (wt%)	EC 1:5 (µS/cm)	% >2mm	%<2mm	strength	rego
DH23	500	313119	6153418	408.42	0	-0.3	1.668777319	37.50	0.35166	0.64834	L	A1=0-10
	500	313119	6153418	408.42	-0.3	-0.6	15.72269908	137.30	0.4946	0.5054	VF	A2=10-30
	500	313119	6153418	408.42	-0.6	-0.9	16.54141124	246.00	0.76068	0.23932	VF	B2=30-150
	500	313119	6153418	408.42	-0.9	-1.2	12.72391706	372.00	0.41781	0.58219	F	C=150-190
	500	313119	6153418	408.42	-1.2	-1.5	9.30261314	361.00	0.05381	0.94619	L/F	
	500	313119	6153418	408.42	-1.5	-1.9	7.866519445	273.00	0.21893	0.78107	L/W	

Drillhole	Distance	easting	northing	Elevation	Depthfrom (m)	Depthto (m)	Moisture (wt%)	EC 1:5 (μS/cm)	% >2mm	%<2mm	strength	rego
DH24	560	313179	6153416	406.89	0	-0.3	11.86251118	67.80	0.45339	0.54661	L/S	A=0-5
	560	313179	6153416	406.89	-0.3	-0.6	12.88649213	113.40	0.37405	0.62595	S	B2=5-60

DH25	580	313200	6153418	406.02	0	-0.3	5.916795827	54.60	0.43115	0.56885	L	A1=0-10
	580	313200	6153418	406.02	-0.3	-0.6	14.5181906	88.90	0.36314	0.63686	S	A2=10-20
	580	313200	6153418	406.02	-0.6	-0.9	13.68668667	108.10	0.3245	0.6755	S	B2=20-100
	580	313200	6153418	406.02	-0.9	-1.25	13.6661396	129.50	0.32817	0.67183	S/R	R=100-120

APPENDIX D: TRANSECT 3 (CANHAM RD) SOIL DATA

Drillhole	distance	easting	northing	elevation at surface	depthfrom (m)	depthto (m)	moisture (wt%)	EC 1:5 (µS/cm)	% >2mm	%<2mm	strength	rego
DH1	0	313973	6153736	420.287	0	-0.3	9.71	55.00	0.06986	0.9347	w	B=0-30
	0	313973	6153736	420.287	-0.3	-0.6	6.96	38.90	0.04547	0.95651	vw	C=30-300
	0	313973	6153736	420.287	-0.6	-0.9	5.22	36.50	0.0264	0.97428	vw	R=300-310
	0	313973	6153736	420.287	-0.9	-1.2	6.27	35.00	0.02143	0.97902	w	
	0	313973	6153736	420.287	-1.2	-1.5	5.91	37.20	0.02793	0.97283	f	
	0	313973	6153736	420.287	-1.5	-2	4.72	36.40	0.02213	0.97835	vw	
	0	313973	6153736	420.287	-2	-2.5	6.32	39.60	0.02917	0.97166	vw	
	0	313973	6153736	420.287	-2.5	-3	7.99	53.70	0.0958	0.91258	w	
	0	313973	6153736	420.287	-3	-3.1	8.21	61.00	0.08525	0.92145	l	

Drillhole	distance	easting	northing	elevation at surface	depthfrom (m)	depthto (m)	moisture (wt%)	EC 1:5 (µS/cm)	% >2mm	%<2mm	strength	rego
DH2	20	313994	6153737	419.974	0	-0.3	16.81	67.00	0.05995	0.94344	f	A=0-10
	20	313994	6153737	419.974	-0.3	-0.6	16.56	50.60	0.00696	0.99309	vf	B= 10-75
	20	313994	6153737	419.974	-0.6	-0.9	12.36	37.20	0.01051	0.9896	f	C =5-680
	20	313994	6153737	419.974	-0.9	-1.2	9.99	34.70	0.00302	0.99699	f	
	20	313994	6153737	419.974	-1.2	-1.5	8.43	35.30	0.0023	0.9977	f	
	20	313994	6153737	419.974	-1.5	-2	7.93	37.10	0.01923	0.98113	s	
	20	313994	6153737	419.974	-2	-2.5	6.90	39.60	0.44951	0.68989	vf	
	20	313994	6153737	419.974	-2.5	-3	9.21	78.50	0.07631	0.9291	f	
	20	313994	6153737	419.974	-3	-3.5	8.78	141.40	0.0032	0.99681	f	
	20	313994	6153737	419.974	-3.5	-4	10.01	307.00	0	1	w	
	20	313994	6153737	419.974	-4	-4.5	10.78	404.00	0.00226	0.99775	w	
	20	313994	6153737	419.974	-4.5	-5	14.59	366.00	0	1	vw	
	20	313994	6153737	419.974	-5	-5.5	15.14	387.00	0	1	vw	
	20	313994	6153737	419.974	-5.5	-6	17.13	519.00	0	1	w	
	20	313994	6153737	419.974	-6	-6.5	20.01	682.00	0	1	w	
	20	313994	6153737	419.974	-6.5	-6.8	17.63	602.00	0	1	w	

Drillhole	distance	easting	northing	elevation at surface	depthfrom (m)	depthto (m)	moisture (wt%)	EC 1:5 (µS/cm)	% >2mm	%<2mm	strength	rego
DH3	40	314014	6153741	417.987	0	-0.3	6.30	72.30	0.17032	0.85446	L	A1=0-15
	40	314014	6153741	417.987	-0.3	-0.6	5.57	34.60	0.10176	0.90764	L	A2=15-60
	40	314014	6153741	417.987	-0.6	-0.9	14.01	67.90	0.11153	0.89966	S	B2=60-140
	40	314014	6153741	417.987	-0.9	-1.2	9.13	67.70	1.25432	0.44359	S	C=140-180
	40	314014	6153741	417.987	-1.2	-1.5	12.45	105.50	0.59159	0.6283	S	
	40	314014	6153741	417.987	-1.5	-1.8	10.11	158.00	0.03316	0.96791	VS	

Drillhole	distance	easting	northing	elevation at surface	depthfrom (m)	depthto (m)	moisture (wt%)	EC 1:5 (µS/cm)	% >2mm	%<2mm	strength	rego
DH4	60	314031	6153740	418.015	0	-0.3	4.86	67.60	0.45662	0.68652	W	A1=25
	60	314031	6153740	418.015	-0.3	-0.6	5.00	40.70	1.62896	0.38038	F	A2=25-40
	60	314031	6153740	418.015	-0.6	-0.9	16.71	59.20	0.08515	0.92153	F	B2=40-140
	60	314031	6153740	418.015	-0.9	-1.2	12.53	56.80	0	1	VF	C=140-180
	60	314031	6153740	418.015	-1.2	-1.5	11.99	103.80	0.01302	0.98714	F	
	60	314031	6153740	418.015	-1.5	-2	11.42	310.00	0.179	0.84817	F	

Drillhole	distance	easting	northing	elevation at surface	depthfrom (m)	depthto (m)	moisture (wt%)	EC 1:5 (µS/cm)	% >2mm	%<2mm	strength	rego
DH5	80	314054	6153739	421.351	0	-0.3	2.84	59.00	0.49466	0.66905	L	A1=0-10
	80	314054	6153739	421.351	-0.3	-0.6	14.16	93.60	0.04919	0.95311	VF	A2=10-20
	80	314054	6153739	421.351	-0.6	-0.9	11.55	79.40	0.32924	0.75231	VF	B2=20-120
	80	314054	6153739	421.351	-0.9	-1.2	9.51	91.30	0.00541	0.99462	VF	C=120-330
	80	314054	6153739	421.351	-1.2	-1.5	8.14	134.90	0.03631	0.96496	F	
	80	314054	6153739	421.351	-1.5	-2	7.71	199.20	0.00955	0.99054	F	
	80	314054	6153739	421.351	-2	-2.5	N/A	N/A	0.01033	0.98978	F	
	80	314054	6153739	421.351	-2.5	-3	7.01	232.20	0.01059	0.98952	L	
	80	314054	6153739	421.351	-3	-3.3	6.94	205.50	0.09236	0.91545	L	

Drillhole	distance	easting	northing	elevation at surface	depthfrom (m)	depthto (m)	moisture (wt%)	EC 1:5 (µS/cm)	% >2mm	%<2mm	strength	rego
DH6	100	314073	6153741	422.712	0	-0.3	4.65	60.70	0.46272	0.68366	F	A1=0-8
	100	314073	6153741	422.712	-0.3	-0.6	11.00	40.70	0.34099	0.74572	VF	A2=8-10
	100	314073	6153741	422.712	-0.6	-0.9	9.70	40.90	0.05344	0.94927	F	B1=10-50
	100	314073	6153741	422.712	-0.9	-1.2	6.76	38.60	0.08879	0.91845	VF	B2=50-80
	100	314073	6153741	422.712	-1.2	-1.5	6.80	46.00	0.87883	0.53225	R	C=80-140

Drillhole	distance	easting	northing	elevation at surface	depthfrom (m)	depthto (m)	moisture (wt%)	EC 1:5 (µS/cm)	% >2mm	%<2mm	strength	rego
DH7	120	314092	6153741	423.767	0	-0.3	2.79	50.70	0.56395	0.63941	L/F	A1=0-5
	120	314092	6153741	423.767	-0.3	-0.6	11.02	51.90	0.19919	0.8339	VF	A2=5-25
	120	314092	6153741	423.767	-0.6	-0.9	10.60	43.20	0.40229	0.71312	VF	B1=25-50
	120	314092	6153741	423.767	-0.9	-1.2	8.05	37.20	0.06464	0.93929	F	B2=50-120
	120	314092	6153741	423.767	-1.2	-1.5	4.81	38.20	0	1	F	C=120-420
	120	314092	6153741	423.767	-1.5	-2	7.51	44.80	0.29455	0.77247	F	R=420
	120	314092	6153741	423.767	-2	-2.5	5.02	45.20	0	1	F	
	120	314092	6153741	423.767	-2.5	-3	8.12	65.10	0.12531	0.88864	R/L	
	120	314092	6153741	423.767	-3	-3.5	5.01	31.60	0	1	R/L	
	120	314092	6153741	423.767	-3.5	-4	4.09	29.10	0	1	W/L	
	120	314092	6153741	423.767	-4	-4.2	4.29	40.50	0	1	R/L	

Drillhole	distance	easting	northing	elevation at surface	depthfrom (m)	depthto (m)	moisture (wt%)	EC 1:5 (µS/cm)	% >2mm	%<2mm	strength	rego
DH8	140	314114	6153745	427.622	0	-0.3	5.54	59.70	0.43395	0.69737	S	B2=0-110
	140	314114	6153745	427.622	-0.3	-0.6	14.82	N/A	0.98336	0.50419	VF	C=110-150
	140	314114	6153745	427.622	-0.6	-0.9	14.10	45.00	0.08445	0.92213	F	R=150-170
	140	314114	6153745	427.622	-0.9	-1.2	11.40	47.70	0.05778	0.94537	VF	
	140	314114	6153745	427.622	-1.2	-1.5	7.10	58.00	0.0853	0.9214	VF/R	
	140	314114	6153745	427.622	-1.5	-1.7	5.11	64.20	0.53864	0.64992	R/L	

Drillhole	distance	easting	northing	elevation at surface	depthfrom (m)	depthto (m)	moisture (wt%)	EC 1:5 (μS/cm)	% >2mm	%<2mm	strength	rego
DH9	160	314131	6153744	430.7424	0	-0.3	15.79	66.00	0.53925	0.64967	VF	B2=0-270
	160	314131	6153744	430.7424	-0.3	-0.6	16.02	37.30	0.04727	0.95486	F	R=270-290
	160	314131	6153744	430.7424	-0.6	-0.9	10.90	37.50	0.49107	0.67066	F	
	160	314131	6153744	430.7424	-0.9	-1.2	15.96	44.30	0.09413	0.91397	VF	
	160	314131	6153744	430.7424	-1.2	-1.5	14.64	50.50	0.41831	0.70507	F	
	160	314131	6153744	430.7424	-1.5	-2	16.01	63.00	0.19768	0.83495	F	
	160	314131	6153744	430.7424	-2	-2.5	15.93	74.40	0.22543	0.81604	S	
	160	314131	6153744	430.7424	-2.5	-2.9	12.55	204.80	0.51331	0.6608	F/R	

Drillhole	distance	easting	northing	elevation at surface	depthfrom (m)	depthto (m)	moisture (wt%)	EC 1:5 (μS/cm)	% >2mm	%<2mm	strength	rego
DH10	180	314149	6153746	433.146	0	-0.3	9.03	54.00	0.43228	0.69819	W/F	A1=0-10
	180	314149	6153746	433.146	-0.3	-0.6	15.54	45.20	0.14775	0.87127	VF	A2=10-17
	180	314149	6153746	433.146	-0.6	-0.9	9.13	44.90	0.25697	0.79557	VF	B2=17-300
	180	314149	6153746	433.146	-0.9	-1.2	15.48	50.10	0.08923	0.91808	VF	R=300-310
	180	314149	6153746	433.146	-1.2	-1.5	15.08	51.30	0.30855	0.7642	VF	
	180	314149	6153746	433.146	-1.5	-2	14.48	55.30	0.16401	0.8591	VF	
	180	314149	6153746	433.146	-2	-2.5	13.54	63.90	0.0488	0.95347	VF	
	180	314149	6153746	433.146	-2.5	-3.1	10.97	65.60	0.27187	0.78624	L/R	

Drillhole	distance	easting	northing	elevation at surface	depthfrom (m)	depthto (m)	moisture (wt%)	EC 1:5 (μS/cm)	% >2mm	%<2mm	strength	rego
DH11	200	314169	6153746	434.817	0	-0.3	0.95	33.10	0.78282	0.56091	L	
	200	314169	6153746	434.817	-0.3	-0.6	19.01	73.50	0.13346	0.88225	W	
	200	314169	6153746	434.817	-0.6	-0.9	17.06	65.50	0.37265	0.72852	F	
	200	314169	6153746	434.817	-0.9	-1.2	16.12	67.80	0.26127	0.79285	VF	
	200	314169	6153746	434.817	-1.2	-1.6	17.09	93.60	0.79208	0.55801	VF	

Drillhole	distance	easting	northing	elevation at surface	depthfrom (m)	depthto (m)	moisture (wt%)	EC 1:5 (µS/cm)	% >2mm	%<2mm	strength	rego
DH12	220	314190	6153746	437.27	0	-0.3	1.55	37.60	0.27566	0.78391	L	A2=0-15
	220	314190	6153746	437.27	-0.3	-0.6	2.84	30.80	0.69828	0.58883	L/W	B1=15-50
	220	314190	6153746	437.27	-0.6	-0.9	12.06	36.40	0.56138	0.64046	W	B2=50-280
	220	314190	6153746	437.27	-0.9	-1.2	12.62	56.60	0.89556	0.52755	F	R=280-290
	220	314190	6153746	437.27	-1.2	-1.5	14.86	71.20	0.17696	0.84965	VF	
	220	314190	6153746	437.27	-1.5	-2	16.88	89.40	0.39317	0.71779	F	
	220	314190	6153746	437.27	-2	-2.5	17.15	100.60	0.31429	0.76087	VF	
	220	314190	6153746	437.27	-2.5	-2.9	15.00	110.60	0.29963	0.76945	L/W	

Drillhole	distance	easting	northing	elevation at surface	depthfrom (m)	depthto (m)	moisture (wt%)	EC 1:5 (µS/cm)	% >2mm	%<2mm	strength	rego
DH13	240	314209	6153746	441.417	0	-0.3	1.42	55.30	0.65261	0.6051	L	A=0-30
	240	314209	6153746	441.417	-0.3	-0.65	1.28	36.30	0.96627	0.50858	R/L	B=30-60
												R=60-65

Drillhole	distance	easting	northing	elevation at surface	depthfrom (m)	depthto (m)	moisture (wt%)	EC 1:5 (µS/cm)	% >2mm	%<2mm	strength	rego
DH14	260	314228	6153748	444.798	0	-0.4	1.05	62.50	0.8517	0.54004	L/R	A=0-30

Drillhole	distance	easting	northing	elevation at surface	depthfrom (m)	depthto (m)	moisture (wt%)	EC 1:5 (µS/cm)	% >2mm	%<2mm	strength	rego
DH15	280	314247	6153750	446.613	0	-0.3	0.98	44.50	0.84191	0.54291	L	A/B=0-55
	280	314247	6153750	446.613	-0.3	-0.55	1.94	40.90	0.11334	0.8982	L	R=55

Drillhole	distance	easting	northing	elevation at surface	depthfrom (m)	depthto (m)	moisture (wt%)	EC 1:5 (µS/cm)	% >2mm	%<2mm	strength	rego
DH16	300	314268	6153749	447.992	0	-0.3	2.37	44.80	0.6851	0.59344	L	A=0-15
	300	314268	6153749	447.992	-0.3	-0.5	2.05	40.90	0.64145	0.60922	R	C=15-45
												R=45-50

Drillhole	distance	easting	northing	elevation at surface	depthfrom (m)	depthto (m)	moisture (wt%)	EC 1:5 (µS/cm)	% >2mm	%<2mm	strength	rego
DH17	320	314285	6153745	447.774	0	-0.3	1.40	31.50	1.64844	0.37758	L	A=1-10
	320	314285	6153745	447.774	-0.3	-0.65	3.03	36.60	0.58436	0.63117	L/R	C/R=10-65

Drillhole	distance	easting	northing	elevation at surface	depthfrom (m)	depthto (m)	moisture (wt%)	EC 1:5 (µS/cm)	% >2mm	%<2mm	strength	rego
DH18	340	314304	6153748	446.499	0	-0.3	2.05	49.10	0.82392	0.54827	L	A=0-20
	340	314304	6153748	446.499	-0.3	-0.6	6.32	38.70	1.02674	0.4934	VW	B/C=20-60
	340	314304	6153748	446.499	-0.6	-0.75	8.41	43.30	0.3715	0.72913	W	R=60-75